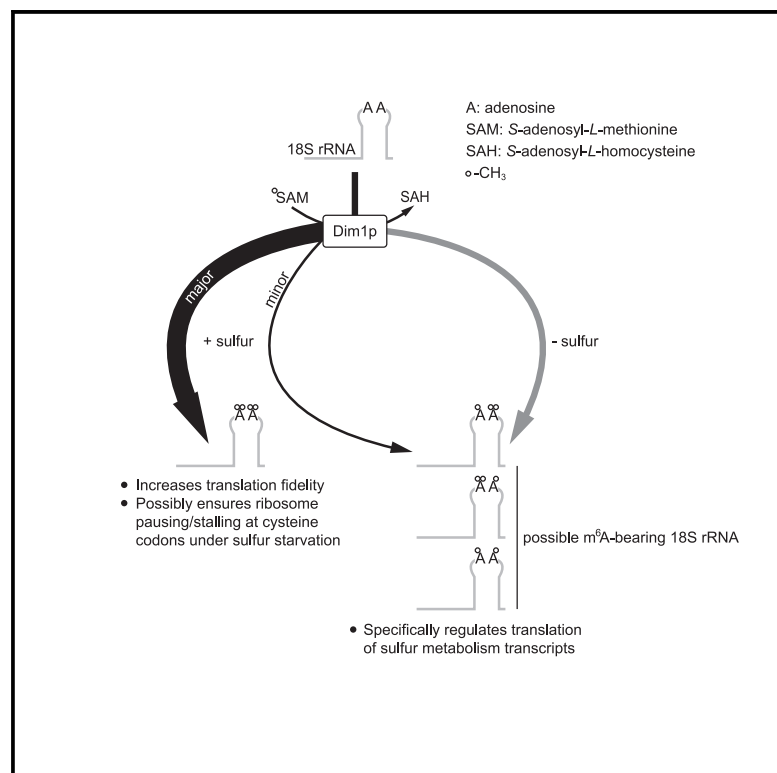


Regulation of translation by methylation multiplicity of 18S rRNA

Graphical Abstract



Authors

Kuanqing Liu, Daniel A. Santos, Jeffrey A. Hussmann, Yun Wang, Benjamin M. Sutter, Jonathan S. Weissman, Benjamin P. Tu

Correspondence

benjamin.tu@utsouthwestern.edu

In brief

Ribosome heterogeneity has become increasingly evident. Liu et al. report an example in the form of rRNA methylation. They show two conserved adenosines in the 18S rRNA are modified with varying numbers of methyl groups. Differentially methylated ribosomes translate differently, suggesting methylation multiplicity as a mechanism to regulate translation.

Highlights

- Two conserved adenosines in the 18S rRNA can be modified as either m⁶A or m⁶₂A
- m⁶A levels increase under sulfur starvation in yeast and mammalian cell lines
- m⁶A-bearing ribosomes translate distinctly from m⁶₂A-bearing ribosomes
- Loss of methylation impairs translation fidelity and ribosome pausing/stalling



Report

Regulation of translation
by methylation multiplicity of 18S rRNAKuanqing Liu,¹ Daniel A. Santos,² Jeffrey A. Hussmann,^{2,3} Yun Wang,¹ Benjamin M. Sutter,¹ Jonathan S. Weissman,^{2,4,5} and Benjamin P. Tu^{1,6,*}¹Department of Biochemistry, University of Texas Southwestern Medical Center, Dallas, TX, USA²Department of Cellular and Molecular Pharmacology, University of California, San Francisco, San Francisco, CA, USA³Department of Microbiology and Immunology, University of California, San Francisco, San Francisco, CA, USA⁴Howard Hughes Medical Institute, University of California, San Francisco, San Francisco, CA, USA⁵Present address: Whitehead Institute for Biomedical Research, Massachusetts Institute of Technology, Cambridge, MA, USA⁶Lead contact*Correspondence: benjamin.tu@utsouthwestern.edu<https://doi.org/10.1016/j.celrep.2021.108825>

SUMMARY

***N*⁶-methyladenosine (m⁶A) is a conserved ribonucleoside modification that regulates many facets of RNA metabolism. Using quantitative mass spectrometry, we find that the universally conserved tandem adenosines at the 3' end of 18S rRNA, thought to be constitutively di-methylated (m⁶₂A), are also mono-methylated (m⁶A). Although present at substoichiometric amounts, m⁶A at these positions increases significantly in response to sulfur starvation in yeast cells and mammalian cell lines. Combining yeast genetics and ribosome profiling, we provide evidence to suggest that m⁶A-bearing ribosomes carry out translation distinctly from m⁶₂A-bearing ribosomes, featuring a striking specificity for sulfur metabolism genes. Our work thus reveals methylation multiplicity as a mechanism to regulate translation.**

INTRODUCTION

RNA, despite its simple composition, is ornamented with more than 150 distinct modifications (Boccaletto et al., 2018). Curiously, ~40% of them involve methylation (<https://iimcb.genesilico.pl/modomics/>), an alkylation reaction that covalently adds a methyl group to a ribonucleoside. Methylation is an energetically expensive process, requiring an energy input equivalent to the hydrolysis of ~13 ATP molecules (Atkinson, 1977). From an evolutionary perspective, this implies that methylation likely confers functional importance. However, except for a few well-characterized examples, many RNA methylation events remain functionally enigmatic (Motorin and Helm, 2011).

Of all methylated ribonucleosides, only a handful have been conserved across all three domains of life (Motorin and Helm, 2011), two prime examples of which are mono-methylated *N*⁶-methyladenosine (m⁶A) and di-methylated *N*⁶-methyladenosine (m⁶₂A). Despite their structural resemblance (one versus two methyl groups at the *N*⁶ position of the adenine ring), m⁶A and m⁶₂A are distinct modifications with respect to their spatial distribution and synthesis. The m⁶A modification was initially discovered in mammalian mRNA (Desrosiers et al., 1974) and subsequently in other RNA species, including rRNA, tRNA, and small nuclear RNA (snRNA) (Yue et al., 2015). In accordance with its promiscuous residencies, several m⁶A methyltransferases targeting different RNA substrates have been identified and characterized (Bokar et al., 1994, 1997; Clancy et al., 2002; Liu et al., 2014; Ma et al., 2019; Pendleton et al., 2017; van Tran et al., 2019), which enabled the functional interrogation

of m⁶A. At the molecular level, m⁶A is known to regulate many facets of RNA metabolism, such as mRNA stability and translation efficiency (TE) (Wang et al., 2014, 2015; Zhou et al., 2015), microRNA (miRNA) processing and maturation (Alarcón et al., 2015a, 2015b), RNA-protein interaction (Liu et al., 2015), and phase separation (Ries et al., 2019). At the cellular level, m⁶A has been implicated in pluripotency (Geula et al., 2015), heat shock response (Zhou et al., 2015), viral infection (Gokhale et al., 2016; Kennedy et al., 2016), and development (Clancy et al., 2002; Zhao et al., 2017). These findings reinforce the notion that addition of a simple methyl group can profoundly affect RNA metabolism and cellular physiology.

In contrast to m⁶A, m⁶₂A has an extremely confined distribution. With a few exceptions, it is found universally at two adjacent adenosines (A1781 and A1782 in *Saccharomyces cerevisiae*) near the 3' end of the small subunit (SSU) rRNA (Rife, 2009; Van Knippenberg et al., 1984). This region forms a highly conserved hairpin loop (helix 45), and the tandem m⁶₂A modifications reside at the apex of this loop, which situates them close to the ribosome decoding site (DCS) (Sharma and Lafontaine, 2015). Despite their remarkable conservation and occupation of a structurally important position within the ribosome, the functional importance of these tandem m⁶₂A modifications remains incompletely understood.

Here, we report our serendipitous discovery that the m⁶₂A methyltransferase Dim1p is capable of modifying the conserved tandem adenosines with a single methyl group (i.e., m⁶A). Although present at low stoichiometry, m⁶A increases significantly during sulfur starvation in yeast cells and mammalian



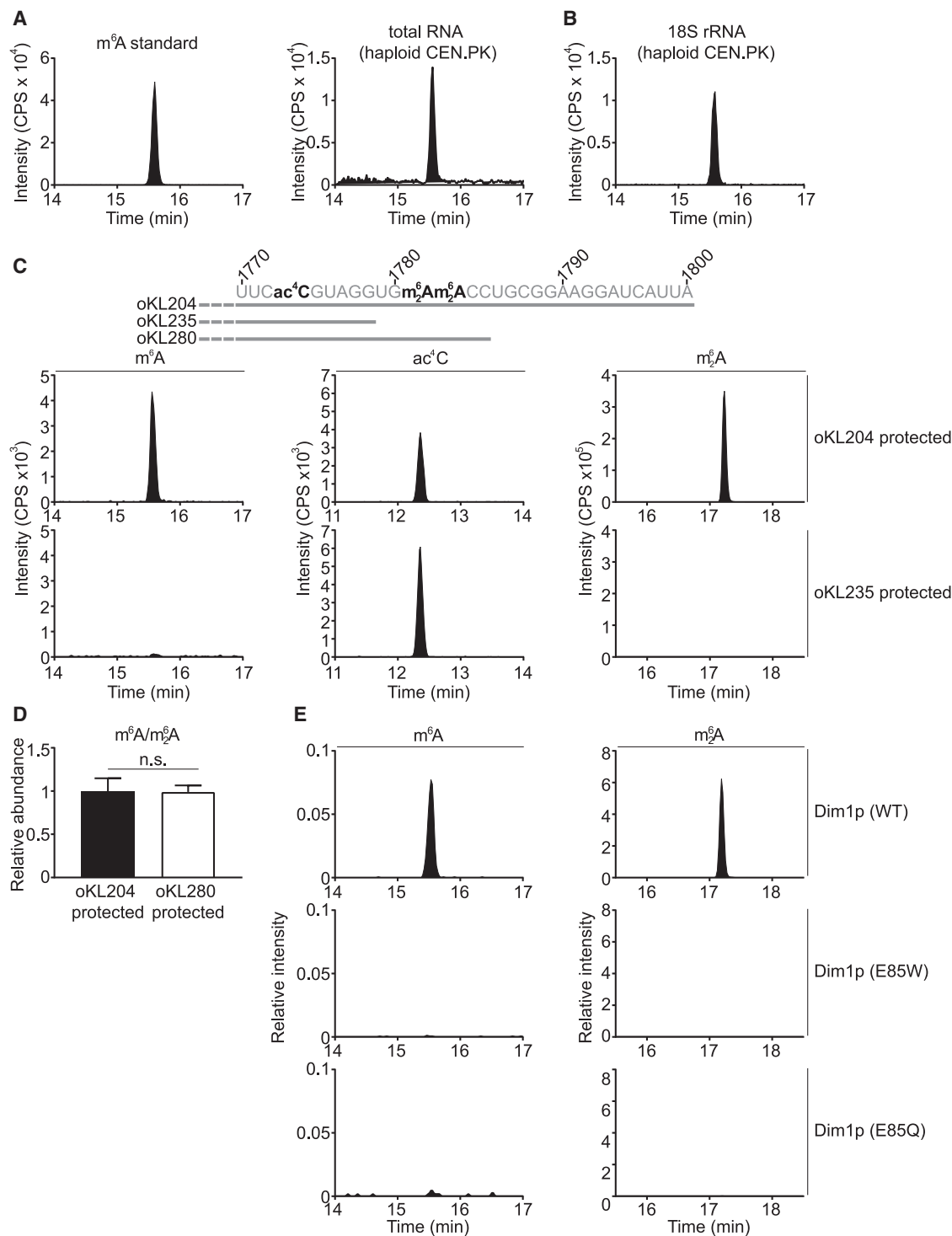


Figure 1. m⁶A is a bona fide modification located at A1781 and/or A1782 of 18S rRNA

(A) Detection of m⁶A in total RNA from vegetatively growing haploid *S. cerevisiae*.

(B) m⁶A is detected in 18S rRNA of vegetatively growing haploid *S. cerevisiae* (strain: CEN.PK).

(C) m⁶A is located in the last 22 nucleotides of 18S rRNA. ac⁴C, N⁴-acetylcytidine; m₂A, N⁶, N⁶-dimethyladenosine. See [Data S1](#) for other regions of 18S rRNA surveyed using the MBN protection assay.

(legend continued on next page)

cell lines. Ribosome profiling experiments further indicate that m⁶A-bearing ribosomes carry out translation distinctly from m⁶₂A-bearing ribosomes, featuring a striking specificity for sulfur metabolism genes. Our work thus suggests that methylation multiplicity of these tandem adenosines functions as a mechanism to regulate translation.

RESULTS

Identification of m⁶A as a bona fide modification at A1781/A1782 in yeast 18S rRNA

Contrary to its prevalence in mammalian cells (Yue et al., 2015), m⁶A in budding yeast cells is present only in mRNA from sporulating diploid cells (Agarwala et al., 2012; Bodi et al., 2010; Clancy et al., 2002). Accordingly, one might expect little m⁶A in the sporulation-deficient haploid cells. Surprisingly, using quantitative liquid chromatography coupled to tandem mass spectrometry, we could readily detect m⁶A in total RNA isolated from haploid cells grown in a synthetic defined (SD) medium (Figures 1A and S1A). Consistent with previous studies (Agarwala et al., 2012; Bodi et al., 2010; Clancy et al., 2002), poly(A)⁺ RNA was essentially devoid of m⁶A (Figure S1B), except in sporulating diploid cells (Figure S1C). Subsequent RNA fractionation revealed the presence of m⁶A in 18S rRNA (Figures 1B and S1D), 25S rRNA (Figure S1E), and small RNA (Figure S1F). However, m⁶A from the latter two sources is likely derived from N¹-methyladenosine (m¹A) via Dimroth rearrangement (Engel, 1975; Macon and Wolfenden, 1968), because loss of the corresponding m¹A methyltransferase or methyltransferases eliminated both m¹A and m⁶A (Figures S1E and S1F). Therefore, only m⁶A detected in 18S rRNA appears to be a bona fide modification. m⁶A is a substoichiometric modification, with ~4% of 18S rRNA on average harboring one m⁶A in haploid yeast cells grown in SD medium.

To precisely map m⁶A in 18S rRNA, we performed a mung bean nuclease (MBN) protection assay (Figure S2A). As validation, we isolated a fragment of yeast 18S rRNA corresponding to the region from 601 to 660 and detected the expected 2'-O-methyladenosine (A_m) (Figure S2B). We next scanned the entire 18S rRNA and found that m⁶A was located within the last 22 nucleotides (nt) (Figure 1C; Data S1). Using a DNA oligo that only partially protects this 22-nt region (Figure 1C), we pinpointed m⁶A to A1781 and/or A1782 of 18S rRNA (Figure 1D). However, due to technical difficulties, we could not further distinguish between these two positions. Nevertheless, an ¹⁵N-tracing experiment showed that m⁶A in 18S rRNA was derived from cultured yeast, not from contamination during sample preparation (Figure S2C). Altogether, these results indicate that m⁶A is a bona fide modification that maps to A1781 and/or A1782 of 18S rRNA, a site also known to accommodate the conserved tandem m⁶₂A modifications.

The co-occupation of m⁶A and m⁶₂A prompted us to speculate that the m⁶₂A methyltransferase Dim1p (Lafontaine et al., 1994) might also be responsible for installing m⁶A. To test this hypothesis, we created a mutant Dim1p by changing the glutamic acid at 85 (E85) to alanine, which reportedly abolishes its methyltransferase activity (Pulicherla et al., 2009). As expected, we found little m⁶₂A in 18S rRNA from the E85A mutant, but surprisingly, we could still detect m⁶A, albeit at slightly reduced amounts (Figure S2D). In the structure of the Dim1 homolog from *Methanocaldococcus jannaschii*, the glutamic acid at 59 (equivalent to E85 in *S. cerevisiae* Dim1p) is within hydrogen-bonding distance to the substrate S-adenosyl-L-methionine (SAM) (Figure S2E) (O'Farrell et al., 2010). Substitution of glutamic acid with alanine might destabilize, but might not eliminate, SAM binding. By contrast, swapping glutamic acid with a bulkier residue might be more effective at disrupting SAM binding through physical hindrance. Indeed, changing the glutamic acid to tryptophan resulted in complete loss of m⁶₂A and m⁶A (Figure 1E), confirming that Dim1p is responsible for both modifications. Furthermore, a highly conservative change of glutamic acid to glutamine inactivated Dim1p, because no m⁶A or m⁶₂A was detected in 18S rRNA of the E85Q mutant (Figure 1E).

m⁶A levels increase specifically and significantly in response to sulfur starvation

The unexpected presence of m⁶A in yeast 18S rRNA raises the question of its biological significance. To this end, we first tested whether m⁶A levels might change according to growth conditions. Deprivation of carbon, nitrogen, or phosphate had little impact on m⁶A levels (Figure 2A). By contrast, sulfate starvation caused a significant increase of m⁶A (Figure 2A), without eliciting apparent changes in amounts of other methylated nucleosides in 18S rRNA (Figure S3A). These observations indicate that m⁶A levels respond specifically to sulfate availability, a notion that is reinforced by the periodic changes of m⁶A in response to sulfate fluctuations (Figure 2B). A stable isotope-tracing experiment further demonstrated that under sulfate starvation, most m⁶A was derived from *de novo* synthesis (Figure 2C), whereas only a minority of m⁶₂A was newly synthesized (Figure S3B). Moreover, this starvation response is not specific for sulfate, because deprivation of methionine or SAM, two reduced sulfur sources, also increased m⁶A levels (Figures 2D and 2E). Supplying cells with S-adenosyl-L-homocysteine (SAH), a product formed following transfer of the methyl group from SAM, was sufficient to increase m⁶A levels even in the presence of sulfate (Figure 2F). Without a sulfur source, the impact of SAH on m⁶A levels was even more pronounced (Figure 2G). Lastly, using the MBN protection assay, we found that HeLa, HEK293T, and 3T3 cells cultured with methionine contained very low levels of m⁶A, only slightly above our detection limit, compared with yeast cells (Figure S3C). By contrast, methionine starvation led to a significant

(D) m⁶A is located at A1781 and/or A1782 of 18S rRNA. The peak area of m⁶A was first normalized to that of m⁶₂A, and the m⁶A/m⁶₂A ratio was then normalized to the fragment protected by oKL204. Mean ± SD (n = 7 biological replicates). The p value was calculated using unpaired two-tailed Student's t test, assuming equal variances.

(E) m⁶₂A methyltransferase Dim1p is responsible for the m⁶A modification in yeast 18S rRNA. p > 0.05 (n.s.).

CPS, counts per second.

See also Figures S1 and S2 and Data S1.

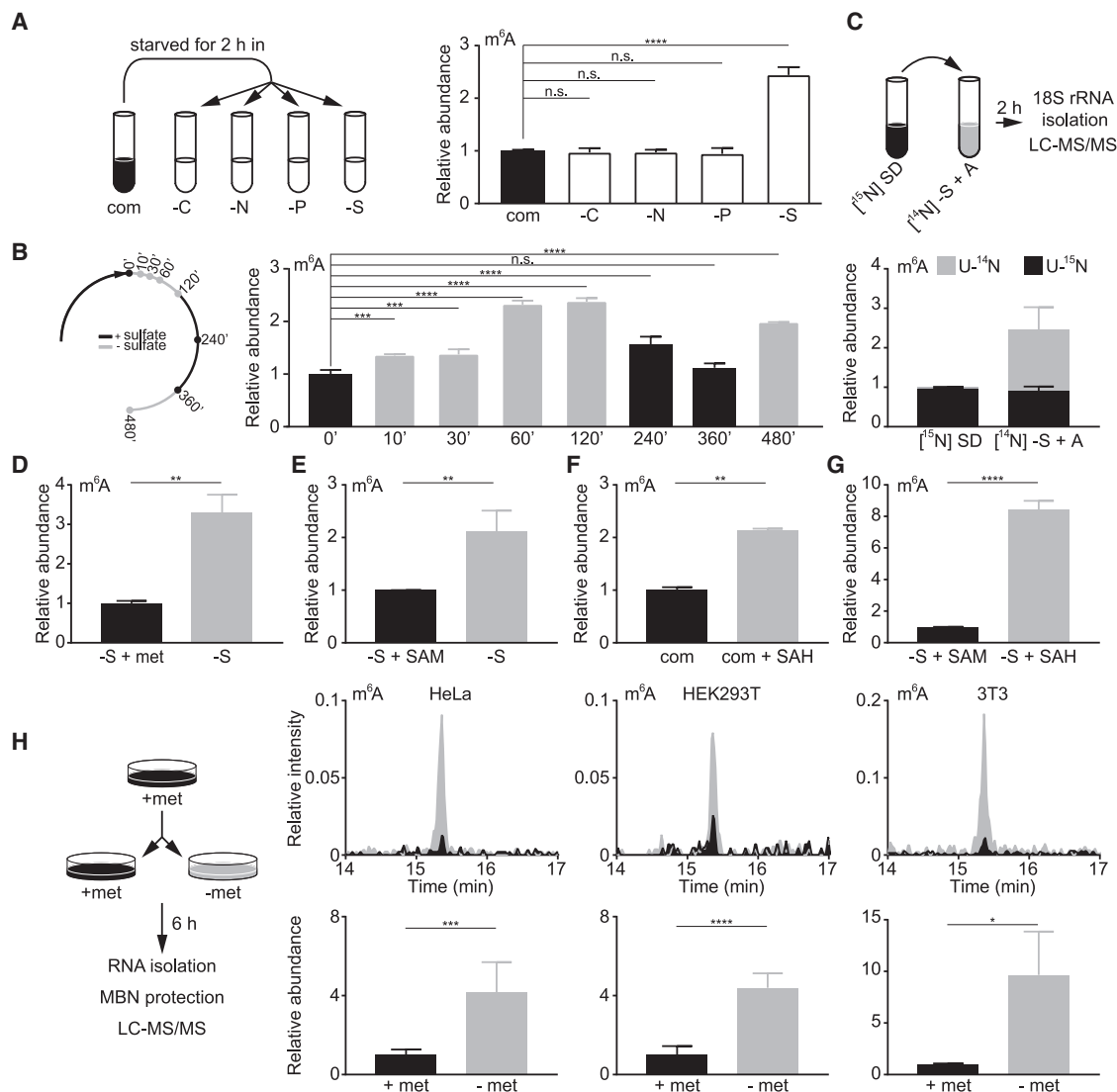


Figure 2. Sulfur starvation increases m⁶A levels in 18S rRNA in yeast cells and mammalian cell lines

(A) m⁶A levels in 18S rRNA increase specifically under sulfate starvation. com, complete medium; -C, carbon starvation; -N, nitrogen starvation; -P, phosphate starvation; -S, sulfate starvation. Mean ± SD (n = 3 biological replicates).

(B) Changes in m⁶A levels in response to sulfate availability. Mean ± SD (n = 2–3 biological replicates).

(C) Increased m⁶A under sulfate starvation is synthesized de novo. Cells were fully labeled in [¹⁵N] SD and starved in [¹⁴N] sulfur-free medium + 50 mg L⁻¹ adenine ([¹⁴N] -S + A) for 2 h. Peak areas of [U-¹⁴N] and [U-¹⁵N] ac⁴C were combined to normalize the differentially labeled m⁶A. Normalized abundance was further divided by that of preswitch samples. Mean ± SD (n = 3 biological replicates).

(D and E) Starvation of methionine (D) and SAM (E) increases m⁶A levels in 18S rRNA. Mean ± SD (n = 3 biological replicates). Methionine (D) and SAM (E) were supplemented at 1 and 0.5 mM, respectively. Data for -S + SAM in (E) were also used in (G).

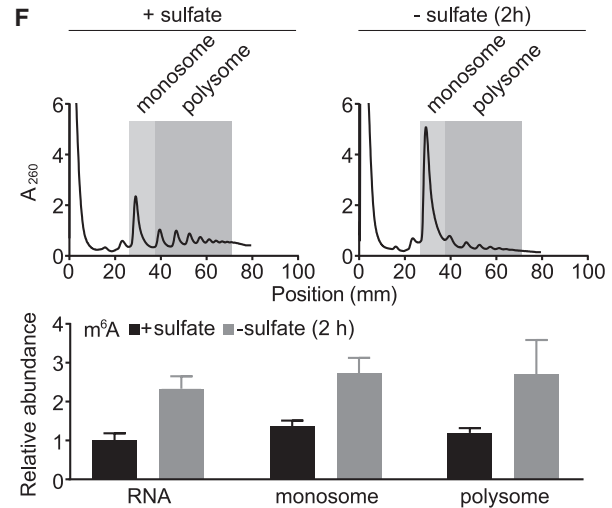
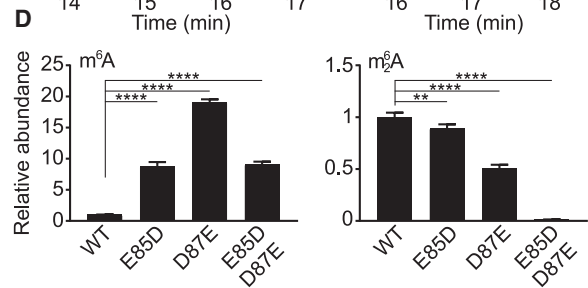
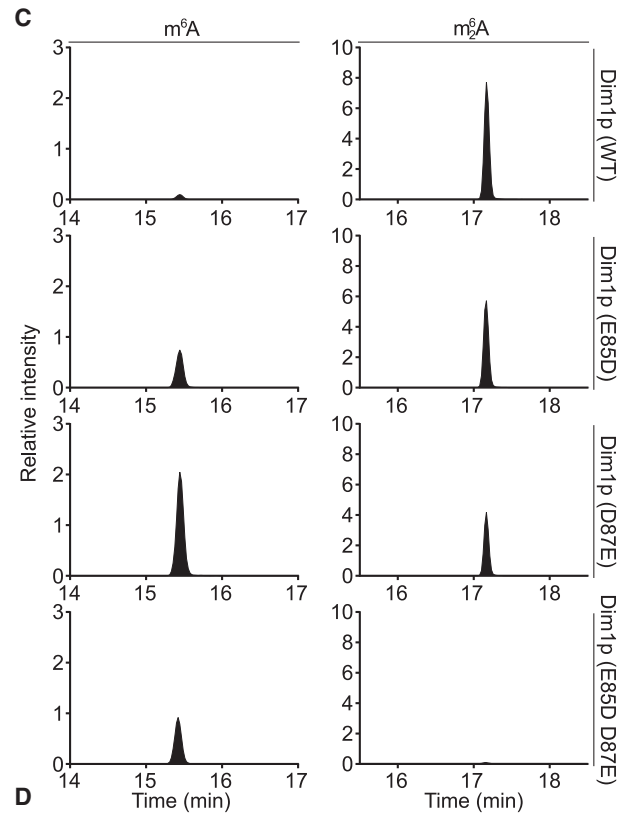
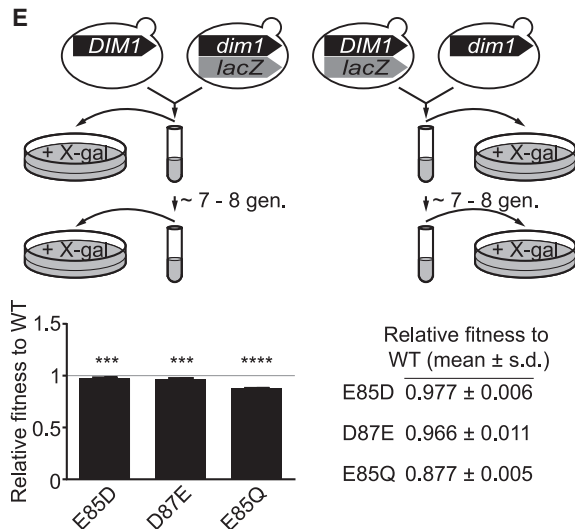
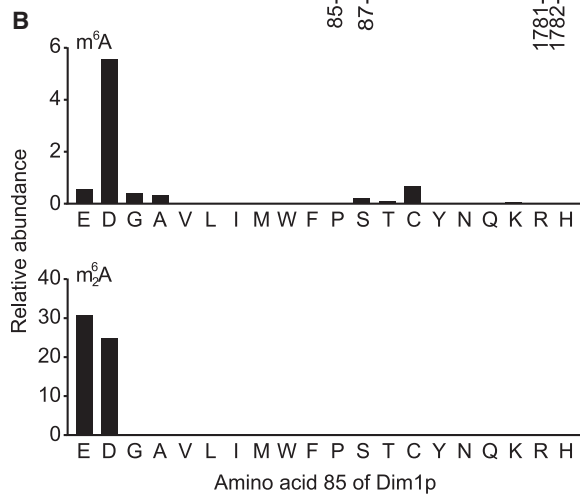
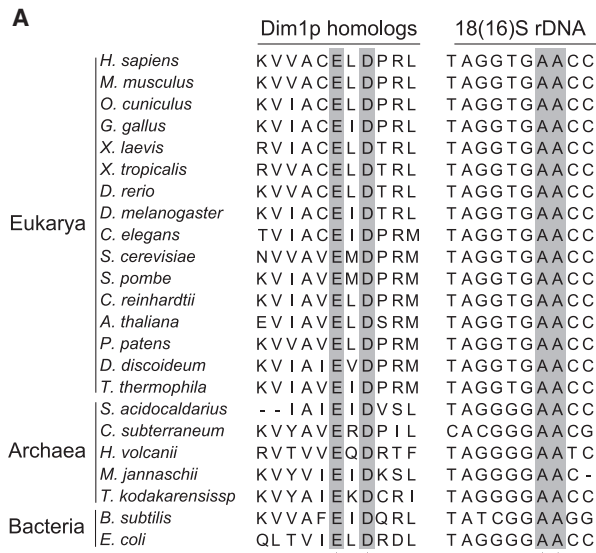
(F) SAH increases m⁶A levels in 18S rRNA. Mean ± SD (n = 2 biological replicates).

(G) SAH enhances the impact of SAM starvation on increasing m⁶A levels in 18S rRNA. SAM and SAH were used at 0.5 mM. Mean ± SD (n = 3 biological replicates).

(H) Methionine starvation increases m⁶A levels at the 3' end of mammalian 18S rRNA. MBN protection assay was performed to specifically examine m⁶A in the last 37 nucleotides of mammalian 18S rRNA. Top panels are representative chromatograms, and bottom panels are quantification results. Mean ± SD (n = 3–7 biological replicates). Chromatograms were normalized to the peak area of ac⁴C to allow comparison between samples. The peak area of m⁶A was first normalized to that of ac⁴C and to samples with methionine.

Ordinary one-way analysis of variance (ANOVA) and Dunnett's multiple comparison test with a single pooled variance were performed to calculate the p values for (A) and (B), and unpaired two-tailed Student's t test, assuming equal variances, was used for (D)–(H). p > 0.05 (n.s.), *p < 0.05, **p < 0.01, ***p < 0.001, ****p < 0.0001.

See also Figure S3.



(legend on next page)

increase of m⁶A in all three cell lines (Figure 2H), suggesting that both yeast and mammalian cells sense sulfur starvation to increase m⁶A in their 18S rRNA. These observations also imply that m⁶A might be functionally important under sulfur starvation.

m⁶A and m⁶₂A in 18S rRNA are not functionally equivalent

Investigating the functional role of m⁶A necessitates a mutant Dim1p that ideally installs only m⁶₂A, but not m⁶A. Sequence alignment from 20 phylogenetically diverse species revealed two universally conserved residues, E85 and D87, in Dim1 homologs, as well as the GAA triplet in SSU rDNA (18S rDNA or 16S rDNA), in which the two adenosines are modified as m⁶A or m⁶₂A (Figure 3A). Inspired by the E85A mutant (Figure S2D), we sought to systematically mutate the glutamic acid to encompass all possible changes at the 85 position. Substitution with small amino acids, e.g., glycine and serine, eliminated m⁶₂A but largely spared m⁶A (Figure 3B). By contrast, replacement with bulky amino acids inactivated Dim1p (Figure 3B). Surprisingly, a conservative change of glutamic acid to aspartic acid led to an approximately nine-fold increase of m⁶A and a commensurate decrease of m⁶₂A (Figures 3B–3D). A reciprocal change at the 87 position (D87E) resulted in even more pronounced elevation of m⁶A (Figures 3C and 3D). Simultaneous introduction of the E85D and D87E substitutions appeared to convert Dim1p into a mono-methyltransferase (Figures 3C and 3D). None of these mutants were able to boost m⁶A levels in response to sulfate starvation (Figure S3D). Collectively, these observations suggest that the E85 and D87 residues of Dim1p are critical for determining methylation multiplicity at A1781/A1782 of 18S rRNA and for relaying a deficiency in sulfur availability to an increase in m⁶A levels.

Although our search for an m⁶₂A-only Dim1p was unsuccessful, we found the E85D and D87E mutants useful for inferring the functions of m⁶A at A1781/A1782. The remarkable conservation of E85 and D87 in Dim1 homologs suggests that these two residues are so crucial that few changes were tolerated during evolution. Consistent with this idea, mutating these two residues, even in the form of conservative changes such as E85D and D87E, invariably reduced cellular fitness (Figure 3E). Because the abundance of Dim1p was not obviously affected by these mutations (Figure S3E), one likely explanation for the preservation of E85 and D87 is to maintain high stoichiometry of m⁶₂A and to relay sulfur availability to m⁶A levels. This interpretation

would further imply that m⁶A and m⁶₂A at A1781/A1782 may not be functionally equivalent.

Regulation of translation by m⁶A in 18S rRNA

Given the proximity of m⁶A and m⁶₂A to the ribosome peptidyl site (P site) (Figure S4A) (Hussain et al., 2014; Tesina et al., 2019) and the DCS (Sharma and Lafontaine, 2015), we speculated that the number of methyl groups might affect translation differentially. To test this hypothesis, we first verified that m⁶A-bearing ribosomes are translation competent (Figures 3F and S4B). Next, we performed polysome profiling to qualitatively examine translation under methionine-replete and methionine-starvation conditions. Three strains were compared: wild type (WT) (~3% m⁶A with methionine and ~10% m⁶A without methionine), the D87E mutant (~80% m⁶A irrespective of methionine availability), and the E85Q mutant (no detectable m⁶A or m⁶₂A under either condition). With methionine, the D87E mutant was highly similar to WT, whereas the E85Q mutant accumulated higher levels of the large subunit (LSU) (Figure S5A), a manifestation of defective SSU biogenesis. Consistently, the E85Q mutant accumulated slightly less SSU (Figure S5B) and showed mild defects in rRNA processing (Figures S6A and S6B). Dim1p is reportedly required for early pre-rRNA processing at A1 and A2, and its depletion reduces 20S and 27SA pre-rRNA but increases 33/32S and 22S pre-rRNA (Lafontaine et al., 1995). Although the E85Q mutant bore resemblance to Dim1p depletion in rRNA processing, it accumulated rather than decreased 20S pre-rRNA (Figure S6B). This observation would argue against the notion that the E85Q mutation impairs cleavage at A1 and/or A2, because inhibition at either site or both is expected to severely reduce the 20S pre-rRNA. Moreover, it illustrates the challenges in uncoupling the methyltransferase activity of Dim1p from its rRNA processing functions (see Discussion). Nevertheless, without methionine, all three strains exhibited reduced polysomes and concomitant increase of monosomes (Figure S5A), indicative of global repression of translation under methionine starvation. Lastly, both yeast and mammalian cells appeared to restrict ribosome biogenesis when methionine is deficient (Figures S6C and S6D), consistent with a previous report (Wejksnora and Haber, 1974).

We next performed ribosome profiling (Ingolia et al., 2009) to quantitatively examine translation in the three strains under methionine-replete and methionine-starvation conditions

Figure 3. m⁶A and m⁶₂A in 18S rRNA are not functionally equivalent

(A) Partial sequence alignment of Dim1 homologs and 18S (16S) rDNA. Highlighted are E85 and D87 of *S. cerevisiae* Dim1p and the two adenosines modified as m⁶A or m⁶₂A.

(B) E85 is a key determinant of the catalytic activity and methylation multiplicity of Dim1p. Data were acquired from the MBN protection assay using oKL204. Peak areas were normalized to that of ac⁴C. Chromatograms of E (WT), W (E85W), Q (E85Q), and A (E85A) were also presented in Figures 1E and S2D.

(C) E85D and D87E mutations alter the methylation multiplicity of Dim1p. Chromatograms from the MBN protection assay using oKL204 were normalized to the peak area of ac⁴C to allow comparison between samples.

(D) Quantification of m⁶A and m⁶₂A in 18S rRNA from *dim1* mutants. Mean ± SD (n = 3–7 biological replicates). The p values were calculated using ordinary one-way ANOVA and Dunnett's multiple comparison test with a single pooled variance. Data were also used for plotting Figure S3D (prestarvation).

(E) Dim1p E85D, D87E, and E85Q mutants have lower fitness than WT. Mean ± SD (n = 4–6 biological replicates). The p values were calculated using one-sample Student's t test.

(F) m⁶A-bearing ribosomes participate in active translation. The peak area of m⁶A was normalized to that of ac⁴C. Mean ± SD (n = 5–6 biological replicates).

p < 0.01, *p < 0.001, ****p < 0.0001.

See also Figures S3, S4, and S8.

(Figure S7A). Because of its known artifacts (Gerashchenko and Gladyshev, 2014; Hussmann et al., 2015; Santos et al., 2019), the translation inhibitor cycloheximide was excluded during sample harvest. Nevertheless, ribosome footprints were enriched in 28- to 29-mers as anticipated (Figure S7B), and excellent reproducibility was observed across ribosome profiling and RNA sequencing (RNA-seq) samples (Figure S7C). At the transcript level, the D87E mutant and WT were indistinguishable, irrespective of methionine availability (Figure S7D; Table S1). By contrast, the transcriptome of the E85Q mutant showed clear differences compared with WT in a methionine-dependent fashion (Figure S7D; Table S1). With methionine, 42 genes were significantly altered in the E85Q mutant (9 upregulated genes and 33 downregulated genes). The downregulated group includes several amino acid metabolism genes (e.g., *MET13*, *MET17*, *STR3*, and *ARG1*), as well as two SSU genes *RPS9A* and *RPS22B* (Figures S7D–S7F; Table S1). Although the *rps9AΔ* and *rps22BΔ* mutants resemble the E85Q mutant in polysome profiles (Figures S7G and S7H), loss of either gene did not lead to the rRNA processing defects observed in the E85Q mutant (Figure S7I). This observation would argue against their low expression as the reason for the defective rRNA processing in the E85Q mutant, although it may still contribute to the under-accumulation of SSU. Nevertheless, without methionine, the transcriptome-wide differences were more prominent between the E85Q mutant and the WT, with 402 genes showing significant changes (Figure S7D). Interestingly, ~54% (120/224) of the upregulated genes in the E85Q mutant encode the ribosome SSU and LSU (Table S1).

We next calculated TE (see STAR methods) to quantitatively examine translation in the three yeast strains. With methionine, 10 genes showed significantly altered TE in the E85Q mutant compared with WT (higher TE: *CST9*, *FIG2*, *STR3*, and *YBR191W-A*; lower TE: *CHA1*, *FIT2*, *FIT3*, *KDX1*, *MAL31*, and *YER186C*) (Figure 4A; Table S2). In the D87E mutant, we identified 16 significantly changed genes (lower TE: *AGP3*, *FIT2*, *FIT3*, *GRX8*, *JLP1*, *MET2*, *MET3*, *MET28*, *MET32*, *MMP1*, *OPT1*, *PDC6*, *SOA1*, *SUL1*, *SUL2*, and *YCT1*) (Figure 4A; Table S2). Remarkably, 12 genes (underlined) are involved in sulfur metabolism, and none of them were significantly changed in the E85Q mutant (Figures 4A–4C; Table S2). This observation suggests that m⁶A at A1781/A1782 of 18S rRNA functions differently from m⁶2A, with a striking specificity for sulfur metabolism genes. It also argues strongly against the notion that the presence of m⁶A at these two conserved adenosines is a fortuitous phenomenon.

These translational differences between the D87E mutant and the WT disappeared under methionine starvation (Figures 4A and 4B; Table S2). Although methionine deprivation generally decreased TE of these sulfur metabolism genes in WT and the E85Q mutant, most of them were translated with higher TE in the D87E mutant (Figure 4D). The only significantly changed gene in the D87E mutant under methionine starvation is *JIP5*, which encodes an essential LSU biogenesis factor (Li et al., 2009) (Figure 4A; Table S2). Methionine starvation drastically reduced TE of *JIP5* in all three strains (Table S3), but the reduction was significantly more pronounced in the D87E mutant (Figure 4A; Table S2). However, methionine starvation led to

significantly more TE changes in the E85Q mutant compared with WT, with 114 genes showing altered TE (55 with higher TE and 59 with lower TE) (Figure 4A; Table S2). Of the genes with lower TE, approximately half (29/59) encode the ribosome SSU and LSU (Table S2).

The E85Q mutant that lacks methylation at A1781/A1782 fails to pause/stall at cysteine codons under methionine starvation

Lastly, we observed that methionine starvation led to strong pausing/stalling at cysteine codons within the ribosome aminoacyl site (A site) in WT and the D87E mutant, which strikingly was absent from the E85Q mutant that lacks both m⁶A and m⁶2A (Figures 5A and 5B). Surprisingly, no pausing at the methionine codon was observed in any of the three strains. Methionine starvation is expected to lower many sulfurous metabolites, including cysteine, which may result in lower cysteinyl-tRNA amounts to cause ribosome pausing/stalling at cysteine codons. Indeed, many sulfurous metabolites plummeted under methionine starvation, but surprisingly, the E85Q mutant was able to maintain higher levels of cysteine, homocysteine, cystathionine, reduced glutathione (GSH), and oxidized glutathione (GSSG) (Figure 5C). Other amino acids were not necessarily increased in the E85Q mutant, suggesting that the higher levels of sulfurous metabolites are not simply due to its slower growth rate (Figures 3E, S8A, and S8B). Nevertheless, although the slightly increased cysteine amounts (~60%) might increase cysteinyl-tRNA to alleviate pausing/stalling, the E85Q mutant still exhibited a substantial reduction of cysteine under methionine starvation (Figure 5C), which led us to consider additional explanations for its lack of pausing/stalling at cysteine codons.

Given that the tandem m⁶2A modifications reside close to the DCS, we speculated that loss of methylation might render ribosomes less sticky at cysteine codons despite limited cysteinyl-tRNA. Perhaps the unmethylated ribosomes are intrinsically prone to errors and could decode cysteine codons using their near-cognate aminoacyl-tRNAs, whose availability is unlikely to be limited by methionine starvation (Figure S8B). To test this hypothesis, we used a luciferase reporter (Figure 5D) (Salas-Marco and Bedwell, 2005) in which a histidine codon (CAC) critical for Firefly luciferase activity is mutated to an arginine encoded by its near-cognate codon CGC. This change severely reduces Firefly luciferase activity, which can be restored if the CGC codon is decoded by histidinyl-tRNA^{GUG}. With this reporter, we found that the E85Q mutant exhibited significantly higher decoding errors than WT and the D87E mutant (Figure 5E), similar to the previously reported E85A mutant (Ghalei et al., 2017). As an important control, we found that disruption of *RPS22B* or *RPS9A* did not increase decoding errors (Figure 5F). Moreover, we deleted the *TSR3* gene, which encodes the aminocarboxypropyl transferase for the N¹-methyl-N³-aminocarboxypropyl-pseudouridine (m¹acp³ψ) modification in yeast 18S rRNA (Meyer et al., 2016). Its deletion causes rRNA processing defects (Li et al., 2009) reminiscent of those observed in the E85Q mutant (Figure S8C). The *tsr3Δ* mutant showed similar decoding fidelity compared with WT cells (Figure 5G). Collectively, these results suggest that the increased decoding errors in the E85Q mutant likely stem from the absence of methylation at A1781/A1782,

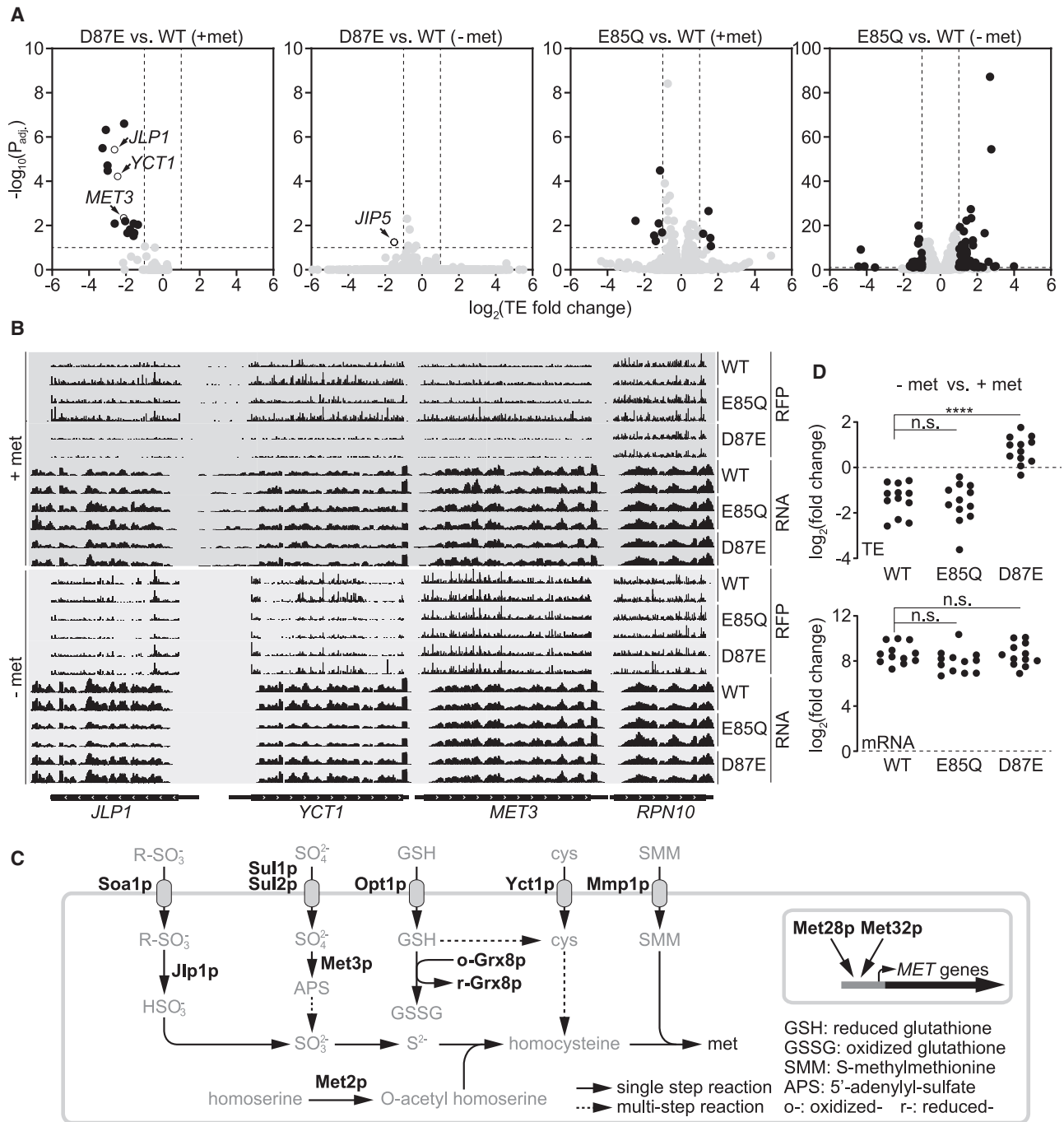


Figure 4. Translational regulation of sulfur metabolism genes via methylation multiplicity

(A) Change of translation efficiency (TE) under methionine-replete and methionine-starvation conditions. A 10% false discovery rate (FDR) ($-\log_{10}(P_{adj}) \geq 1$) and 2-fold change of TE ($\log_2(\text{TE fold change}) \geq 1$ or $\log_2(\text{TE fold change}) \leq -1$) are considered significant, and genes with significantly changed TE are highlighted in black.

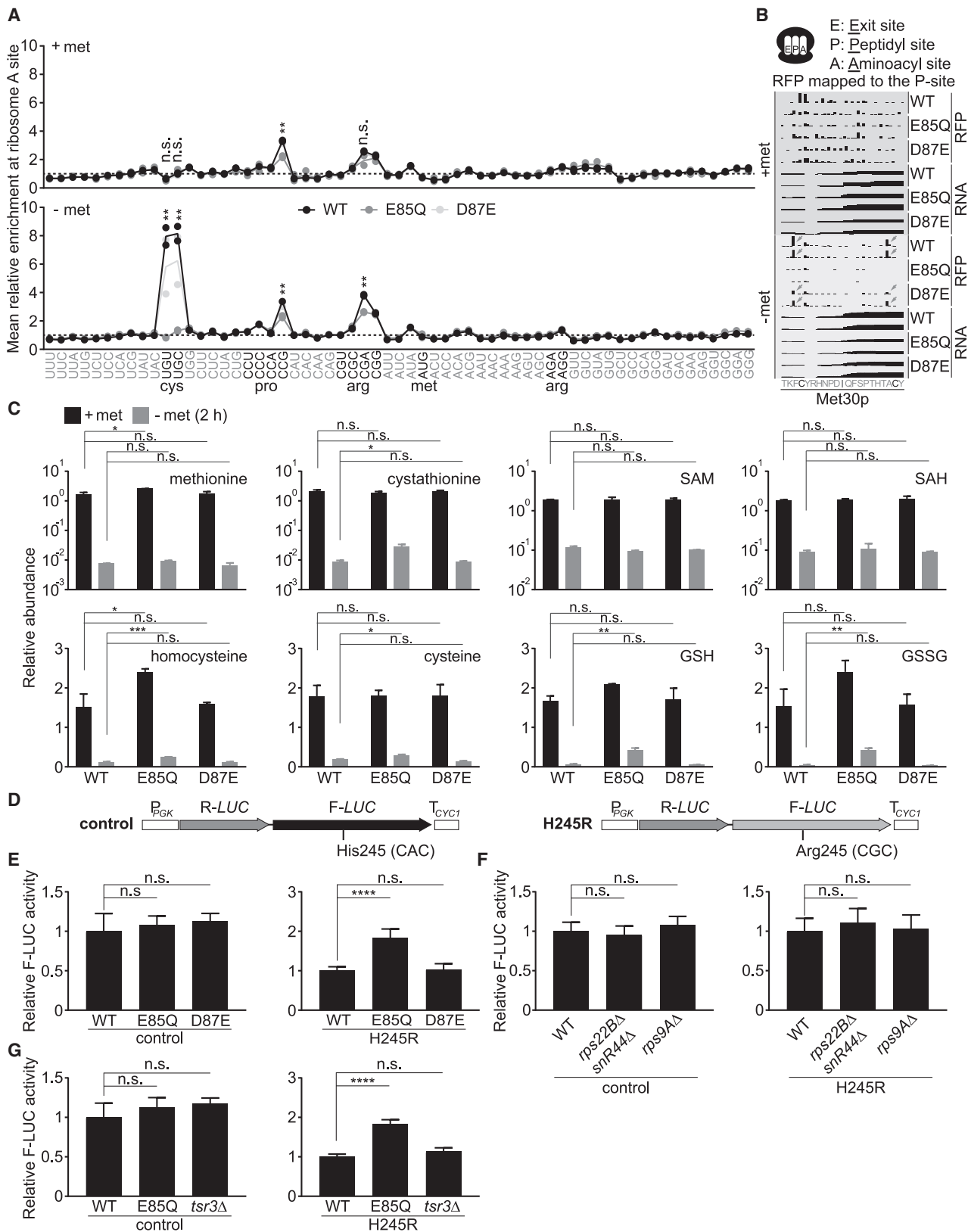
(B) Representative tracks of ribosome footprint (RFP) and mRNA for *JLP1*, *YCT1*, *MET3*, and *RPN10*. Two biological replicates for each genotype are shown, and tracks are comparable only within each RFP or RNA group.

(C) Simplified schematic of yeast sulfur metabolism. Highlighted are proteins whose transcripts are translated with significantly lower TE in the D87E mutant under methionine-replete conditions.

(D) Impact of methionine starvation on TE and mRNA levels of sulfur metabolism genes listed in (C).

The p values were calculated using two-sided Mann-Whitney test. ****p < 0.0001.

See also [Figures S5–S7](#) and [Tables S1, S2, and S3](#).



(legend on next page)

rather than rRNA processing defects. Loss of methylation at these tandem adenosines may facilitate decoding of cysteine codons at the cost of translation fidelity to alleviate pausing/stalling under methionine starvation. This interpretation might also explain the attenuated pausing/stalling at CCG (proline) and CGA (arginine) codons in the E85Q mutant (Figure 5A), because both are rare codons without their cognate tRNAs (Tuller et al., 2010).

DISCUSSION

Methylation multiplicity as a mechanism to diversify ribosomes to regulate translation

Ribosomes have long been perceived as a homogeneous population. However, it has become evident that they may exist as a group of heterogeneous entities, with respect to not only their protein subunit composition but also modifications of these subunits and rRNA (Byrgazov et al., 2013; Dinman, 2016; Genuth and Barna, 2018). Here, we present another example of ribosome heterogeneity in the form of rRNA methylation via methylation multiplicity. The presence of m⁶A at the conserved tandem adenosines in 18S rRNA, together with m⁶₂A, increases the complexity of the SSU. By conducting a comprehensive mutagenesis analysis, we were able to increase m⁶A levels in bulk by introducing an E85D or D87E mutation to Dim1p (Figures 3B–3D). Such conservative changes by a single methylene group (-CH₂) minimize perturbations that could be inadvertently introduced to the cell. Analyses of polysome and ribosome subunit profiles (Figures S5A and S5B), rRNA processing (Figure S6B), the transcriptome (Figure S7D), intracellular metabolites (Figures 5C and S8B), and 18S rRNA modifications (Figure S8D) indicate that the D87E mutant is virtually indistinguishable from WT. Still, this mutant bearing more m⁶A in its ribosomes carries out translation distinctly compared with WT cells, featuring a striking specificity for sulfur metabolism genes and a peculiar dependency on sulfur availability (Figures 4A–4C). It is unclear how this specificity is determined, although all of these genes are heavily induced at the transcriptional level by methionine starvation (Figure 4D; Table S3). Perhaps a *cis*-regulatory element is embedded in their transcripts to confer the specificity, as reported previously (Xue et al., 2015). However, ongoing bioinformatic investigation has yet to identify promising candidates. In addition, *trans*-acting factors (e.g., RNA-binding proteins) might assist in determining the specificity (Leppek et al., 2018).

With respect to the sulfur dependency, two outstanding questions remain. The first concerns how sulfur metabolism transcripts are translated with higher TE in the D87E mutant under methionine starvation (Figure 4D), when global translation is repressed (Figure S5A). One possible explanation is that m⁶A-bearing SSU might function more efficiently using non-canonical translation pathways, e.g., internal ribosome entry site (IRES)-mediated translation, which is known to operate under stress conditions (Gilbert et al., 2007; Holcik and Sonenberg, 2005; Spriggs et al., 2008). Under methionine-replete conditions, m⁶A-bearing SSU might be inefficient at translating sulfur metabolism transcripts using the canonical cap-dependent pathway, perhaps because of the presence of IRES in their 5' untranslated regions. Under methionine starvation, cap-dependent translation may be inhibited because of methionine scarcity. m⁶A-bearing SSU, perhaps with assistance from IRES *trans*-acting factors (King et al., 2010; Komar and Hatzoglou, 2011), might be able to efficiently recognize IRES within these sulfur metabolism transcripts to support their translation during methionine starvation.

The second question concerns the dependency of the TE differences between the WT and the D87E mutant on methionine availability (Figure 4A). Because translation of these sulfur metabolism transcripts is seemingly recalcitrant to methionine deprivation in the D87E mutant (Figure 4D), we speculate that they might be translated predominantly by m⁶A-bearing ribosomes in WT under methionine starvation. A single yeast cell is estimated to contain ~200,000 ribosomes (von der Haar, 2008; Warner, 1999), and a stoichiometry of ~10% would equal ~20,000 m⁶A-bearing ribosomes in methionine-starved WT cells. If the yeast transcriptome comprises ~60,000 mRNA molecules (Zenklusen et al., 2008), there should be sufficient m⁶A-bearing ribosomes for these sulfur metabolism transcripts.

Functional importance of the tandem m⁶₂A modifications

Modified ribonucleosides are prevalent in rRNAs. Because many of them reside in structurally important positions within the ribosome (Sloan et al., 2017), it is perhaps not surprising that rRNA modifications have been shown to play key roles in maintaining translation efficiency and translation accuracy (Baudin-Baillieu et al., 2009; Jack et al., 2011; King et al., 2003; Lafontaine et al., 1998; Liang et al., 2009; Ma et al., 2019; Schosserer et al., 2015). rRNA modifications can also be selectively impactful, because some appear to regulate translation of only a subset of mRNAs, such as rRNA pseudouridylation (Bellodi et al., 2010a,

Figure 5. The E85Q mutation abolishes pausing/stalling at cysteine codons under methionine starvation

- (A) Relative enrichment of ribosomes at each codon under methionine-replete and methionine-starvation conditions. Reads were mapped to the ribosome aminoacyl site (A site). Two biological replicates for each genotype are shown (two circles per genotype), with their average being represented by a solid line. The p values were calculated using unpaired two-tailed Student's t test, assuming equal variances for comparison between WT and the E85Q mutant.
- (B) Representative tracks showing enrichment of ribosomes at two cysteine codons of the *MET30* transcript following methionine starvation.
- (C) Changes in sulfurous metabolites under methionine-replete and methionine-starvation conditions. Mean ± SD (n = 2 biological replicates).
- (D) Schematic of the dual luciferase reporters.
- (E) E85Q mutant has higher decoding errors. Mean ± SD (n = 6 biological replicates).
- (F) Loss of *RPS22B/snR44* or *RPS9A* does not affect decoding fidelity. Mean ± SD (n = 5–11 and n = 7–11 biological replicates for the control and the H245R reporter, respectively).
- (G) rRNA processing defects due to loss of *TSR3* do not increase decoding errors. Mean ± SD (n = 3 biological replicates).
- The p values were calculated using ordinary one-way ANOVA and Dunnett's multiple comparison test with a single pooled variance for (C) and (E)–(G). p > 0.05 (n.s.), *p < 0.05, **p < 0.01, ***p < 0.001, ****p < 0.0001. See also Figures S7 and S8.

2010b; Yoon et al., 2006) and 2'-O-methylation (Basu et al., 2011; Erales et al., 2017; Marcel et al., 2013) in IRES-mediated translation. Moreover, a recent study suggests that m⁶A in *C. elegans* 18S rRNA is important for translating an mRNA involved in lipid oxidation (Lieberman et al., 2020).

Among all known rRNA modifications, the tandem m⁶₂A modifications are remarkably conserved; they are found almost universally at the 3' end of SSU rRNA (Rife, 2009; Van Knippenberg et al., 1984), which situates them close to the ribosome P site (Figure S4A) and the DCS (Sharma and Lafontaine, 2015). Despite their conservation and occupation of a structurally important location, the functional importance of the tandem m⁶₂A modifications remains incompletely understood. One obstacle is that Dim1p (and its homologs) is a dual-function protein required for both m⁶₂A methylation and rRNA processing (Connolly et al., 2008; Lafontaine et al., 1995; Zorbas et al., 2015), and a *dim1* mutant that completely uncouples these two functions has hitherto been elusive (see Limitations of study). A previous study showed that cellular extract from a *dim1-2* mutant was incompetent at translating reporter genes (Lafontaine et al., 1998). Although some defects may result from the loss of m⁶₂A, effects of impaired rRNA processing in the *dim1-2* mutant have not been excluded. In our work, some changes in the E85Q mutant in the ribosome profiling and RNA-seq experiments (Figures 4A and S7D), as well as the growth assays (Figures 3E and S8A), may stem from rRNA processing defects. However, we have performed important controls to rule out defects in SSU biogenesis and rRNA processing as an explanation for the increased decoding errors in the E85Q mutant (Figures 5F and 5G). Therefore, minimally, we conclude that the tandem m⁶₂A modifications are important for maintaining translation fidelity and possibly for pausing/stalling at cysteine codons under methionine starvation.

Limitations of study

Challenges in uncoupling the methyltransferase activity of Dim1p from its rRNA processing functions

Functional interrogation of the tandem m⁶₂A modifications necessitates a *dim1* mutant that uncouples its methyltransferase activity from its rRNA processing functions. Despite significant efforts in previous studies (Connolly et al., 2008; Lafontaine et al., 1998) and our work, such a mutant has yet to be found. An early study in yeast constructed a temperature-sensitive *dim1-2* mutant that is reportedly defective in methylation (Lafontaine et al., 1998). However, this *dim1-2* mutant, containing six substitutions, still exhibits rRNA processing defects and retains some methyltransferase activity for m⁶₂A and perhaps for m⁶A as well (primer extension may not effectively distinguish between m⁶A and A). Similar efforts in *E. coli* were also unsuccessful (Connolly et al., 2008): the tested KsgA^{E66A} (equivalent to Dim1p^{E85A}) might still be partially active based on our findings with Dim1p^{E85A} (Figures 3B and S2D), and importantly it leads to defects in SSU biogenesis and rRNA processing (Connolly et al., 2008). Here, we introduced a highly conservative E85Q mutation to eliminate the methyltransferase activity of Dim1p (Figure 1E), but unfortunately, this E85Q mutant is still defective in SSU biogenesis (Figures S5A and S5B) and rRNA processing (Figure S6B). Recent structural work reveals that the E85A mutation has little impact on the overall conformation of human DIMT1 (Shen et al., 2020), and conceivably, the E85Q mutation

would be expected to be even less disruptive. Still, even such a conservative change leads to rRNA processing defects. With the aforementioned early findings, this led us to speculate that the methyltransferase activity of Dim1p might be involved in rRNA processing, as proposed previously (Connolly et al., 2008).

Therefore, the difficulty in uncoupling the dual functions of Dim1p may limit our interpretation of the ribosome profiling and RNA-seq experiments (Figures 4A and S7D) and of the growth assays (Figures 3E and S8A), because some changes may not stem directly from the loss of methylation. However, we have included important controls to rule out defects in SSU biogenesis and rRNA processing as an explanation for the increased decoding errors in the E85Q mutant (Figures 5F and 5G). In closing, the tandem m⁶₂A modifications are important for ensuring translational fidelity and possibly for pausing/stalling at cysteine codons under methionine starvation. Nonetheless, these and other phenotypes of the E85Q mutant, such as changes in transcript levels or translational efficiency, could be secondary and compensatory because of defects in rRNA processing and/or SSU biogenesis.

STAR★METHODS

Detailed methods are provided in the online version of this paper and include the following:

- KEY RESOURCES TABLE
- RESOURCE AVAILABILITY
 - Lead contact
 - Materials availability
 - Data and code availability
- EXPERIMENTAL MODEL AND SUBJECT DETAILS
 - Yeast strains and growth conditions
 - Mammalian cell lines and growth conditions
- METHOD DETAILS
 - Total RNA isolation
 - RNA fractionation
 - Estimation of stoichiometry of m⁶A in yeast 18S rRNA
 - Mung bean nuclease (MBN) protection assay
 - LC-MS/MS detection of nucleosides
 - LC-MS/MS detection of metabolites
 - Competition assay
 - Dual-luciferase assay
 - Polysome profiling
 - Western blot
 - Northern blot
 - Ribosome profiling
 - Sequencing data analysis
 - Metacodon analysis
- QUANTIFICATION AND STATISTICAL ANALYSIS

SUPPLEMENTAL INFORMATION

Supplemental Information can be found online at <https://doi.org/10.1016/j.celrep.2021.108825>.

ACKNOWLEDGMENTS

We thank Dr. David Bedwell from University of Alabama at Birmingham for the generous gifts of pDB722 and pDB868. We also thank Dr. Juan Manuel

Povedano for critically reading the manuscript and Venkat Malladi at the Bioinformatics Core Facility of UT Southwestern Medical Center for assistance with sequencing data analysis. J.S.W. is supported by the Howard Hughes Medical Institute. D.A.S. is supported by the National Science Foundation (1650113) and Moritz-Heyman Discovery Fellowship. J.A.H. is the Rebecca Ridley Kry Fellow of the Damon Runyon Cancer Research Foundation (DRG-2262-16). B.P.T. is supported by the Welch Foundation (I-1797) and NIH (grants R35GM136370 and R01NS115546).

AUTHOR CONTRIBUTIONS

This study was conceived by K.L. and B.P.T. K.L. conducted all genetics, molecular biology, and mass spectrometry experiments. D.A.S. performed ribosome profiling and RNA-seq, D.A.S. and K.L. analyzed the sequencing data, J.A.H. performed metacodon analysis, Y.W. performed experiments with mammalian cell lines, and B.M.S. performed western blots. K.L. led and conducted all other experiments in this study. Funding support was provided by B.P.T. and J.S.W. The manuscript was written by K.L. and B.P.T. All authors have read and approve the manuscript.

DECLARATION OF INTERESTS

The authors declare no competing interests.

Received: June 2, 2020

Revised: January 4, 2021

Accepted: February 12, 2021

Published: March 9, 2021

SUPPORTING CITATIONS

The following references appear in the supplemental information: Calvo et al. (1999); Gueldener et al. (2002); Keeling et al. (2004); Miller et al. (2013); Taoka et al. (2016); Voth et al. (2001).

REFERENCES

Agarwala, S.D., Blitzblau, H.G., Hochwagen, A., and Fink, G.R. (2012). RNA methylation by the MIS complex regulates a cell fate decision in yeast. *PLoS Genet.* *8*, e1002732.

Alarcón, C.R., Goodarzi, H., Lee, H., Liu, X., Tavazoie, S., and Tavazoie, S.F. (2015a). HNRNPA2B1 is a mediator of m(6)A-dependent nuclear RNA processing events. *Cell* *162*, 1299–1308.

Alarcón, C.R., Lee, H., Goodarzi, H., Halberg, N., and Tavazoie, S.F. (2015b). *N*⁶-methyladenosine marks primary microRNAs for processing. *Nature* *519*, 482–485.

Andersen, T.E., Porse, B.T., and Kirpekar, F. (2004). A novel partial modification at C2501 in *Escherichia coli* 23S ribosomal RNA. *RNA* *10*, 907–913.

Atkinson, D. (1977). Cellular energy metabolism and its regulation (Academic Press), p. 75.

Basu, A., Das, P., Chaudhuri, S., Bevilacqua, E., Andrews, J., Barik, S., Hatzoglou, M., Komar, A.A., and Mazumder, B. (2011). Requirement of rRNA methylation for 80S ribosome assembly on a cohort of cellular internal ribosome entry sites. *Mol. Cell. Biol.* *31*, 4482–4499.

Baudin-Baillieu, A., Fabret, C., Liang, X.H., Piekna-Przybylska, D., Fournier, M.J., and Rousset, J.P. (2009). Nucleotide modifications in three functionally important regions of the *Saccharomyces cerevisiae* ribosome affect translation accuracy. *Nucleic Acids Res.* *37*, 7665–7677.

Bellodi, C., Kopmar, N., and Ruggero, D. (2010a). Deregulation of oncogene-induced senescence and p53 translational control in X-linked dyskeratosis congenita. *EMBO J.* *29*, 1865–1876.

Bellodi, C., Krasnykh, O., Haynes, N., Theodoropoulou, M., Peng, G., Montanaro, L., and Ruggero, D. (2010b). Loss of function of the tumor suppressor DKC1 perturbs p27 translation control and contributes to pituitary tumorigenesis. *Cancer Res.* *70*, 6026–6035.

Boccaletto, P., Machnicka, M.A., Purta, E., Piatkowski, P., Baginski, B., Wirecki, T.K., de Crécy-Lagard, V., Ross, R., Limbach, P.A., Kotter, A., et al. (2018). MODOMICS: a database of RNA modification pathways. 2017 update. *Nucleic Acids Res.* *46* (D1), D303–D307.

Bodi, Z., Button, J.D., Grierson, D., and Fray, R.G. (2010). Yeast targets for mRNA methylation. *Nucleic Acids Res.* *38*, 5327–5335.

Bokar, J.A., Rath-Shambaugh, M.E., Ludwiczak, R., Narayan, P., and Rottman, F. (1994). Characterization and partial purification of mRNA N6-adenosine methyltransferase from HeLa cell nuclei. Internal mRNA methylation requires a multisubunit complex. *J. Biol. Chem.* *269*, 17697–17704.

Bokar, J.A., Shambaugh, M.E., Polayes, D., Matera, A.G., and Rottman, F.M. (1997). Purification and cDNA cloning of the AdoMet-binding subunit of the human mRNA (N6-adenosine)-methyltransferase. *RNA* *3*, 1233–1247.

Brar, G.A., Yassour, M., Friedman, N., Regev, A., Ingolia, N.T., and Weissman, J.S. (2012). High-resolution view of the yeast meiotic program revealed by ribosome profiling. *Science* *335*, 552–557.

Byrgazov, K., Vesper, O., and Moll, I. (2013). Ribosome heterogeneity: another level of complexity in bacterial translation regulation. *Curr. Opin. Microbiol.* *16*, 133–139.

Calvo, O., Cuesta, R., Anderson, J., Gutiérrez, N., García-Barrio, M.T., Hinnebusch, A.G., and Tamame, M. (1999). GCD14p, a repressor of *GCN4* translation, cooperates with Gcd10p and Lhp1p in the maturation of initiator methionyl-tRNA in *Saccharomyces cerevisiae*. *Mol. Cell. Biol.* *19*, 4167–4181.

Castrillo, J.I., Hayes, A., Mohammed, S., Gaskell, S.J., and Oliver, S.G. (2003). An optimized protocol for metabolome analysis in yeast using direct infusion electrospray mass spectrometry. *Phytochemistry* *62*, 929–937.

Clancy, M.J., Shambaugh, M.E., Tipton, C.S., and Bokar, J.A. (2002). Induction of sporulation in *Saccharomyces cerevisiae* leads to the formation of *N*⁶-methyladenosine in mRNA: a potential mechanism for the activity of the *IME4* gene. *Nucleic Acids Res.* *30*, 4509–4518.

Connolly, K., Rife, J.P., and Culver, G. (2008). Mechanistic insight into the ribosome biogenesis functions of the ancient protein KsgA. *Mol. Microbiol.* *70*, 1062–1075.

Desrosiers, R., Friderici, K., and Rottman, F. (1974). Identification of methylated nucleosides in messenger RNA from Novikoff hepatoma cells. *Proc. Natl. Acad. Sci. USA* *71*, 3971–3975.

Dinman, J.D. (2016). Pathways to specialized ribosomes: the Brussels lecture. *J. Mol. Biol.* *428* (10 Pt B), 2186–2194.

Dunn, J.G., and Weissman, J.S. (2016). Plastid: nucleotide-resolution analysis of next-generation sequencing and genomics data. *BMC Genomics* *17*, 958.

Engel, J.D. (1975). Mechanism of the Dimroth rearrangement in adenosine. *Biochem. Biophys. Res. Commun.* *64*, 581–586.

Erales, J., Marchand, V., Panthu, B., Gillot, S., Belin, S., Ghayad, S.E., Garcia, M., Laforêts, F., Marcel, V., Baudin-Baillieu, A., et al. (2017). Evidence for rRNA 2'-O-methylation plasticity: Control of intrinsic translational capabilities of human ribosomes. *Proc. Natl. Acad. Sci. USA* *114*, 12934–12939.

Genuth, N.R., and Bama, M. (2018). The discovery of ribosome heterogeneity and its implications for gene regulation and organismal life. *Mol. Cell* *71*, 364–374.

Geraschenko, M.V., and Gladyshev, V.N. (2014). Translation inhibitors cause abnormalities in ribosome profiling experiments. *Nucleic Acids Res.* *42*, e134.

Geula, S., Moshitch-Moshkovitz, S., Dominissini, D., Mansour, A.A., Kol, N., Salmon-Divon, M., Hershkovitz, V., Peer, E., Mor, N., Manor, Y.S., et al. (2015). m⁶A mRNA methylation facilitates resolution of naïve pluripotency toward differentiation. *Science* *347*, 1002–1006.

Ghalei, H., Trepreau, J., Collins, J.C., Bhaskaran, H., Strunk, B.S., and Karbstein, K. (2017). The ATPase Fap7 tests the ability to carry out translocation-like conformational changes and releases Dim1 during 40S ribosome maturation. *Mol. Cell* *67*, 990–1000.e3.

Gibson, D.G., Young, L., Chuang, R.Y., Venter, J.C., Hutchison, C.A., 3rd, and Smith, H.O. (2009). Enzymatic assembly of DNA molecules up to several hundred kilobases. *Nat. Methods* *6*, 343–345.

- Gilbert, W.V., Zhou, K., Butler, T.K., and Doudna, J.A. (2007). Cap-independent translation is required for starvation-induced differentiation in yeast. *Science* *317*, 1224–1227.
- Gokhale, N.S., McIntyre, A.B.R., McFadden, M.J., Roder, A.E., Kennedy, E.M., Gandara, J.A., Hopcraft, S.E., Quicke, K.M., Vazquez, C., Willer, J., et al. (2016). *N*⁶-methyladenosine in Flaviviridae viral RNA genomes regulates infection. *Cell Host Microbe* *20*, 654–665.
- Gonzalez, B., François, J., and Renaud, M. (1997). A rapid and reliable method for metabolite extraction in yeast using boiling buffered ethanol. *Yeast* *13*, 1347–1355.
- Guldener, U., Heinisch, J., Koehler, G.J., Voss, D., and Hegemann, J.H. (2002). A second set of loxP marker cassettes for Cre-mediated multiple gene knockouts in budding yeast. *Nucleic Acids Res.* *30*, e23.
- Holcik, M., and Sonenberg, N. (2005). Translational control in stress and apoptosis. *Nat. Rev. Mol. Cell Biol.* *6*, 318–327.
- Hussain, T., Llácer, J.L., Fernández, I.S., Munoz, A., Martin-Marcos, P., Savva, C.G., Lorsch, J.R., Hinnebusch, A.G., and Ramakrishnan, V. (2014). Structural changes enable start codon recognition by the eukaryotic translation initiation complex. *Cell* *159*, 597–607.
- Hussmann, J.A., Patchett, S., Johnson, A., Sawyer, S., and Press, W.H. (2015). Understanding biases in ribosome profiling experiments reveals signatures of translation dynamics in yeast. *PLoS Genet.* *11*, e1005732.
- Ingolia, N.T., Ghaemmaghami, S., Newman, J.R., and Weissman, J.S. (2009). Genome-wide analysis *in vivo* of translation with nucleotide resolution using ribosome profiling. *Science* *324*, 218–223.
- Jack, K., Bellodi, C., Landry, D.M., Niederer, R.O., Meskauskas, A., Musalgaonkar, S., Kopmar, N., Krasnykh, O., Dean, A.M., Thompson, S.R., et al. (2011). rRNA pseudouridylation defects affect ribosomal ligand binding and translational fidelity from yeast to human cells. *Mol. Cell* *44*, 660–666.
- Josefsen, K., and Nielsen, H. (2011). Northern blotting analysis. In *RNA: Methods and Protocols*, H. Nielsen, ed. (Humana Press), pp. 87–105.
- Keeling, K.M., Lanier, J., Du, M., Salas-Marco, J., Gao, L., Kaenjak-Angeletti, A., and Bedwell, D.M. (2004). Leaky termination at premature stop codons antagonizes nonsense-mediated mRNA decay in *S. cerevisiae*. *RNA* *10*, 691–703.
- Kennedy, E.M., Bogerd, H.P., Kornepati, A.V., Kang, D., Ghoshal, D., Marshall, J.B., Poling, B.C., Tsai, K., Gokhale, N.S., Horner, S.M., and Cullen, B.R. (2016). Posttranscriptional m⁶A editing of HIV-1 mRNAs enhances viral gene expression. *Cell Host Microbe* *19*, 675–685.
- Kim, D., Pertea, G., Trapnell, C., Pimentel, H., Kelley, R., and Salzberg, S.L. (2013). TopHat2: accurate alignment of transcriptomes in the presence of insertions, deletions and gene fusions. *Genome Biol.* *14*, R36.
- King, T.H., Liu, B., McCully, R.R., and Fournier, M.J. (2003). Ribosome structure and activity are altered in cells lacking snoRNPs that form pseudouridines in the peptidyl transferase center. *Mol. Cell* *11*, 425–435.
- King, H.A., Cobbold, L.C., and Willis, A.E. (2010). The role of IRES *trans*-acting factors in regulating translation initiation. *Biochem. Soc. Trans.* *38*, 1581–1586.
- Komar, A.A., and Hatzoglou, M. (2011). Cellular IRES-mediated translation: the war of ITAFs in pathophysiological states. *Cell Cycle* *10*, 229–240.
- Korolev, K.S., Müller, M.J., Karahan, N., Murray, A.W., Hallatschek, O., and Nelson, D.R. (2012). Selective sweeps in growing microbial colonies. *Phys. Biol.* *9*, 026008.
- Lafontaine, D., Delcour, J., Glasser, A.L., Desgrès, J., and Vandenhaute, J. (1994). The *DIM1* gene responsible for the conserved m³Am⁶Am²A dimethylation in the 3'-terminal loop of 18 S rRNA is essential in yeast. *J. Mol. Biol.* *241*, 492–497.
- Lafontaine, D., Vandenhaute, J., and Tollervey, D. (1995). The 18S rRNA dimethylase Dim1p is required for pre-ribosomal RNA processing in yeast. *Genes Dev.* *9*, 2470–2481.
- Lafontaine, D.L., Preiss, T., and Tollervey, D. (1998). Yeast 18S rRNA dimethylase Dim1p: a quality control mechanism in ribosome synthesis? *Mol. Cell Biol.* *18*, 2360–2370.
- Laxman, S., Sutter, B.M., Wu, X., Kumar, S., Guo, X., Trudgian, D.C., Mirzaei, H., and Tu, B.P. (2013). Sulfur amino acids regulate translational capacity and metabolic homeostasis through modulation of tRNA thiolation. *Cell* *154*, 416–429.
- Leppek, K., Das, R., and Barna, M. (2018). Functional 5' UTR mRNA structures in eukaryotic translation regulation and how to find them. *Nat. Rev. Mol. Cell Biol.* *19*, 158–174.
- Li, Z., Lee, I., Moradi, E., Hung, N.J., Johnson, A.W., and Marcotte, E.M. (2009). Rational extension of the ribosome biogenesis pathway using network-guided genetics. *PLoS Biol.* *7*, e1000213.
- Liang, X.H., Liu, Q., and Fournier, M.J. (2009). Loss of rRNA modifications in the decoding center of the ribosome impairs translation and strongly delays pre-rRNA processing. *RNA* *15*, 1716–1728.
- Lieberman, N., O'Brown, Z.K., Earl, A.S., Boulias, K., Gerashchenko, M.V., Wang, S.Y., Fritsche, C., Fady, P.E., Dong, A., Gladyshev, V.N., and Greer, E.L. (2020). N⁶-adenosine methylation of ribosomal RNA affects lipid oxidation and stress resistance. *Sci. Adv.* *6*, eaaz4370.
- Liu, N., Parisien, M., Dai, Q., Zheng, G., He, C., and Pan, T. (2013). Probing N⁶-methyladenosine RNA modification status at single nucleotide resolution in mRNA and long noncoding RNA. *RNA* *19*, 1848–1856.
- Liu, J., Yue, Y., Han, D., Wang, X., Fu, Y., Zhang, L., Jia, G., Yu, M., Lu, Z., Deng, X., et al. (2014). A METTL3-METTL14 complex mediates mammalian nuclear RNA N⁶-adenosine methylation. *Nat. Chem. Biol.* *10*, 93–95.
- Liu, N., Dai, Q., Zheng, G., He, C., Parisien, M., and Pan, T. (2015). N⁶-methyladenosine-dependent RNA structural switches regulate RNA-protein interactions. *Nature* *518*, 560–564.
- Longtine, M.S., McKenzie, A., 3rd, Demarini, D.J., Shah, N.G., Wach, A., Brachat, A., Philippsen, P., and Pringle, J.R. (1998). Additional modules for versatile and economical PCR-based gene deletion and modification in *Saccharomyces cerevisiae*. *Yeast* *14*, 953–961.
- Love, M.I., Huber, W., and Anders, S. (2014). Moderated estimation of fold change and dispersion for RNA-seq data with DESeq2. *Genome Biol.* *15*, 550.
- Ma, H., Wang, X., Cai, J., Dai, Q., Natchiar, S.K., Lv, R., Chen, K., Lu, Z., Chen, H., Shi, Y.G., et al. (2019). N⁶-Methyladenosine methyltransferase ZCCHC4 mediates ribosomal RNA methylation. *Nat. Chem. Biol.* *15*, 88–94.
- Macon, J.B., and Wolfenden, R. (1968). 1-Methyladenosine. Dimroth rearrangement and reversible reduction. *Biochemistry* *7*, 3453–3458.
- Marcel, V., Ghayad, S.E., Belin, S., Therizols, G., Morel, A.P., Solano-González, E., Vendrell, J.A., Hacot, S., Mertani, H.C., Albaret, M.A., et al. (2013). p53 acts as a safeguard of translational control by regulating fibrillarin and rRNA methylation in cancer. *Cancer Cell* *24*, 318–330.
- Mašek, T., Valásek, L., and Pospíšek, M. (2011). Polysome analysis and RNA purification from sucrose gradients. *Methods Mol. Biol.* *703*, 293–309.
- McGlincy, N.J., and Ingolia, N.T. (2017). Transcriptome-wide measurement of translation by ribosome profiling. *Methods* *126*, 112–129.
- Meyer, B., Wurm, J.P., Sharma, S., Immer, C., Pogoryelov, D., Kötter, P., Lafontaine, D.L., Wöhnert, J., and Entian, K.D. (2016). Ribosome biogenesis factor Tsr3 is the aminocarboxypropyl transferase responsible for 18S rRNA hypermodification in yeast and humans. *Nucleic Acids Res.* *44*, 4304–4316.
- Mikkelsen, M.D., Buron, L.D., Salomonsen, B., Olsen, C.E., Hansen, B.G., Mortensen, U.H., and Halkier, B.A. (2012). Microbial production of indolylglucosinolate through engineering of a multi-gene pathway in a versatile yeast expression platform. *Metab. Eng.* *14*, 104–111.
- Miller, A.W., Befort, C., Kerr, E.O., and Dunham, M.J. (2013). Design and use of multiplexed chemostat arrays. *J. Vis. Exp.* *72*, e50262.
- Motorin, Y., and Helm, M. (2011). RNA nucleotide methylation. *Wiley Interdiscip. Rev. RNA* *2*, 611–631.
- O'Farrell, H.C., Musayev, F.N., Scarsdale, J.N., and Rife, J.P. (2010). Binding of adenosine-based ligands to the MjDim1 rRNA methyltransferase: implications for reaction mechanism and drug design. *Biochemistry* *49*, 2697–2704.

- Peifer, C., Sharma, S., Watzinger, P., Lamberth, S., Kötter, P., and Entian, K.D. (2013). Yeast Rrp8p, a novel methyltransferase responsible for m¹A 645 base modification of 25S rRNA. *Nucleic Acids Res.* *41*, 1151–1163.
- Pendleton, K.E., Chen, B., Liu, K., Hunter, O.V., Xie, Y., Tu, B.P., and Conrad, N.K. (2017). The U6 snRNA m⁶A methyltransferase METTL16 regulates SAM synthetase intron retention. *Cell* *169*, 824–835.e14.
- Pulicherla, N., Pogorzala, L.A., Xu, Z., O Farrell, H.C., Musayev, F.N., Scarsdale, J.N., Sia, E.A., Culver, G.M., and Rife, J.P. (2009). Structural and functional divergence within the Dim1/KsgA family of rRNA methyltransferases. *J. Mol. Biol.* *397*, 884–893.
- Ries, R.J., Zaccara, S., Klein, P., Olarerin-George, A., Namkoong, S., Pickering, B.F., Patil, D.P., Kwak, H., Lee, J.H., and Jaffrey, S.R. (2019). m⁶A enhances the phase separation potential of mRNA. *Nature* *571*, 424–428.
- Rife, J.P. (2009). Roles of the ultra-conserved ribosomal RNA methyltransferase KsgA in ribosome biogenesis. In *DNA and RNA Modification Enzymes: Structure, Mechanism, Function and Evolution*, H. Grosjean, ed. (Landes Bioscience), pp. 512–526.
- Salas-Marco, J., and Bedwell, D.M. (2005). Discrimination between defects in elongation fidelity and termination efficiency provides mechanistic insights into translational readthrough. *J. Mol. Biol.* *348*, 801–815.
- Sankar, T.S., Wastuwidyaningtyas, B.D., Dong, Y., Lewis, S.A., and Wang, J.D. (2016). The nature of mutations induced by replication–transcription collisions. *Nature* *535*, 178–181.
- Santos, D.A., Shi, L., Tu, B.P., and Weissman, J.S. (2019). Cycloheximide can distort measurements of mRNA levels and translation efficiency. *Nucleic Acids Res.* *47*, 4974–4985.
- Schossner, M., Minois, N., Angerer, T.B., Amring, M., Dellago, H., Harreither, E., Calle-Perez, A., Pircher, A., Gerstl, M.P., Pfeifenberger, S., et al. (2015). Methylation of ribosomal RNA by NSUN5 is a conserved mechanism modulating organismal lifespan. *Nat. Commun.* *6*, 6158.
- Sharma, S., and Lafontaine, D.L.J. (2015). ‘View from a bridge’: A new perspective on eukaryotic rRNA base modification. *Trends Biochem. Sci.* *40*, 560–575.
- Sharma, S., Watzinger, P., Kötter, P., and Entian, K.D. (2013). Identification of a novel methyltransferase, Bmt2, responsible for the N-1-methyl-adenosine base modification of 25S rRNA in *Saccharomyces cerevisiae*. *Nucleic Acids Res.* *41*, 5428–5443.
- Shen, H., Stoute, J., and Liu, K.F. (2020). Structural and catalytic roles of the human 18S rRNA methyltransferases DIMT1 in ribosome assembly and translation. *J. Biol. Chem.* *295*, 12058–12070.
- Sloan, K.E., Warda, A.S., Sharma, S., Entian, K.D., Lafontaine, D.L.J., and Bohnsack, M.T. (2017). Tuning the ribosome: The influence of rRNA modification on eukaryotic ribosome biogenesis and function. *RNA Biol.* *14*, 1138–1152.
- Spriggs, K.A., Stoneley, M., Bushell, M., and Willis, A.E. (2008). Re-programming of translation following cell stress allows IRES-mediated translation to predominate. *Biol. Cell* *100*, 27–38.
- Tafforeau, L., Zorbas, C., Langhendries, J.L., Mullineux, S.T., Stamatopoulou, V., Mullier, R., Wacheul, L., and Lafontaine, D.L. (2013). The complexity of human ribosome biogenesis revealed by systematic nucleolar screening of Pre-rRNA processing factors. *Mol. Cell* *51*, 539–551.
- Taoka, M., Nobe, Y., Yamaki, Y., Yamauchi, Y., Ishikawa, H., Takahashi, N., Nakayama, H., and Isobe, T. (2016). The complete chemical structure of *Saccharomyces cerevisiae* rRNA: partial pseudouridylation of U2345 in 25S rRNA by snoRNA snR9. *Nucleic Acids Res.* *44*, 8951–8961.
- Tesina, P., Heckel, E., Cheng, J., Fromont-Racine, M., Buschauer, R., Kater, L., Beatrix, B., Berninghausen, O., Jacquier, A., Becker, T., and Beckmann, R. (2019). Structure of the 80S ribosome-Xrn1 nuclease complex. *Nat. Struct. Mol. Biol.* *26*, 275–280.
- Tu, B.P., Mohler, R.E., Liu, J.C., Dombek, K.M., Young, E.T., Synovec, R.E., and McKnight, S.L. (2007). Cyclic changes in metabolic state during the life of a yeast cell. *Proc. Natl. Acad. Sci. USA* *104*, 16886–16891.
- Tuller, T., Carmi, A., Vestsgian, K., Navon, S., Dorfan, Y., Zaborske, J., Pan, T., Dahan, O., Furman, I., and Pilpel, Y. (2010). An evolutionarily conserved mechanism for controlling the efficiency of protein translation. *Cell* *141*, 344–354.
- van Dijken, J.P., Bauer, J., Brambilla, L., Duboc, P., Francois, J.M., Gancedo, C., Giuseppini, M.L., Heijnen, J.J., Hoare, M., Lange, H.C., et al. (2000). An interlaboratory comparison of physiological and genetic properties of four *Saccharomyces cerevisiae* strains. *Enzyme Microb. Technol.* *26*, 706–714.
- Van Knippenberg, P.H., Van Kimmenade, J.M., and Heus, H.A. (1984). Phylogeny of the conserved 3′ terminal structure of the RNA of small ribosomal subunits. *Nucleic Acids Res.* *12*, 2595–2604.
- van Tran, N., Ernst, F.G.M., Hawley, B.R., Zorbas, C., Ulryck, N., Hackert, P., Bohnsack, K.E., Bohnsack, M.T., Jaffrey, S.R., Graille, M., and Lafontaine, D.L.J. (2019). The human 18S rRNA m⁶A methyltransferase METTL5 is stabilized by TRMT112. *Nucleic Acids Res.* *47*, 7719–7733.
- von der Haar, T. (2008). A quantitative estimation of the global translational activity in logarithmically growing yeast cells. *BMC Syst. Biol.* *2*, 87.
- Voth, W.P., Richards, J.D., Shaw, J.M., and Stillman, D.J. (2001). Yeast vectors for integration at the HO locus. *Nucleic Acids Res.* *29*, E59.
- Wang, X., Lu, Z., Gomez, A., Hon, G.C., Yue, Y., Han, D., Fu, Y., Parisien, M., Dai, Q., Jia, G., et al. (2014). N⁶-methyladenosine-dependent regulation of messenger RNA stability. *Nature* *505*, 117–120.
- Wang, X., Zhao, B.S., Roundtree, I.A., Lu, Z., Han, D., Ma, H., Weng, X., Chen, K., Shi, H., and He, C. (2015). N⁶-methyladenosine modulates messenger RNA translation efficiency. *Cell* *161*, 1388–1399.
- Warner, J.R. (1999). The economics of ribosome biosynthesis in yeast. *Trends Biochem. Sci.* *24*, 437–440.
- Wejksnora, P.J., and Haber, J.E. (1974). Methionine-dependent synthesis of ribosomal ribonucleic acid during sporulation and vegetative growth of *Saccharomyces cerevisiae*. *J. Bacteriol.* *120*, 1344–1355.
- Xue, S., Tian, S., Fujii, K., Kladwang, W., Das, R., and Barna, M. (2015). RNA regulons in Hox 5′ UTRs confer ribosome specificity to gene regulation. *Nature* *517*, 33–38.
- Yoon, A., Peng, G., Brandenburger, Y., Zollo, O., Xu, W., Rego, E., and Ruggero, D. (2006). Impaired control of IRES-mediated translation in X-linked dyskeratosis congenita. *Science* *312*, 902–906.
- Yue, Y., Liu, J., and He, C. (2015). RNA N⁶-methyladenosine methylation in post-transcriptional gene expression regulation. *Genes Dev.* *29*, 1343–1355.
- Zenkhusen, D., Larson, D.R., and Singer, R.H. (2008). Single-RNA counting reveals alternative modes of gene expression in yeast. *Nat. Struct. Mol. Biol.* *15*, 1263–1271.
- Zhao, B.S., Wang, X., Beadell, A.V., Lu, Z., Shi, H., Kuuspalu, A., Ho, R.K., and He, C. (2017). m⁶A-dependent maternal mRNA clearance facilitates zebrafish maternal-to-zygotic transition. *Nature* *542*, 475–478.
- Zhou, J., Wan, J., Gao, X., Zhang, X., Jaffrey, S.R., and Qian, S.B. (2015). Dynamic m⁶A mRNA methylation directs translational control of heat shock response. *Nature* *526*, 591–594.
- Zorbas, C., Nicolas, E., Wacheul, L., Huvelle, E., Heurgué-Hamad, V., and Lafontaine, D.L. (2015). The human 18S rRNA base methyltransferases DIMT1L and WBSR22-TRMT112 but not rRNA modification are required for ribosome biogenesis. *Mol. Biol. Cell* *26*, 2080–2095.

STAR★METHODS

KEY RESOURCES TABLE

REAGENT or RESOURCE	SOURCE	IDENTIFIER
Antibodies		
Mouse monoclonal anti-FLAG antibody	Sigma	Cat#F1804
Rabbit polyclonal anti-G6pdh antibody	Sigma	Cat#A9521
Rabbit polyclonal anti-Rpn10 antibody	Abcam	Cat#ab98843
Chemicals, peptides, and recombinant proteins		
Nuclease P1 from <i>Penicillium citrinum</i>	Sigma	Cat#N8630
Phusion® High-Fidelity DNA Polymerase	New England Biolabs	Cat#M0530S
DpnI	New England Biolabs	Cat#R0176S
RNase A	Lucigen	Cat#MRNA092
Phosphodiesterase I from <i>Crotalus atrox</i>	Sigma	Cat#P4506
Alkaline phosphatase calf intestinal	New England Biolabs	Cat#M0290
Mung bean nuclease	New England Biolabs	Cat#M0250L
Critical commercial assays		
RPMI-1640	GIBCO	Cat#A14517-01
DMEM	GIBCO	Cat#21013-024
Fetal bovine serum	Sigma	Cat#F6178
Yeast nitrogen base without amino acids	BD Difco	Cat#BD233520
complete EDTA-free protease inhibitor cocktail tablets	Roche	Cat#11873580001
Chemiluminescent nucleic acid detection module kit	Thermo Fisher	Cat#89880
D-Tube Dialyzer Mini (MWCO 6-8 kDa)	EMD Millipore	Cat#71-504-3
Dual-Luciferase® Reporter assay system	Promega	Cat#E1910
NucleoSpin® gel and PCR clean-up kit	Takara	Cat#740609
PureLink miRNA isolation kit	Invitrogen	Cat#K157001
NuPAGE 4-12% polyacrylamide Bis-Tris Gels	Invitrogen	Cat#WG1403BX10
Ribo-Zero Gold for yeast	Illumina	Cat#MRZY1306
Dynabeads mRNA purification kit	Invitrogen	Cat#61006
Deposited data		
Raw and analyzed data	This paper	GEO: GSE142528
Experimental models: cell lines		
HeLa	ATCC	Cat#CCL-2
Lenti-X 293T	Takara	Cat#632180
3T3	ATCC	Cat#CRL-1658
Experimental models: organisms/strains		
CEN.PK MATa	van Dijken et al., 2000	NA
CEN.PK MATa/ α	van Dijken et al., 2000	NA
S288C MAT α	ATCC	Cat#204508
W303 MATa	Korolev et al., 2012	NA
A full list of yeast mutant strains is provided in Table S4	NA	NA
Oligonucleotides		
A full list of oligos is provided in Table S4	NA	NA
Recombinant DNA		
A full list of plasmids is provided in Table S4	NA	NA

(Continued on next page)

Continued

REAGENT or RESOURCE	SOURCE	IDENTIFIER
Software and algorithms		
Analyst software package	AB SCIEX	Versions 1.6.2 or 1.6.3
Image Lab	Bio-Rad	Version 6.0
ImageJ	National Institutes of Health	Version 1.50e
Integrative Genomics Viewer	Broad Institute	2.8.0
GraphPad Prism	GraphPad Software	Versions 6, 7, 8, and 9

RESOURCE AVAILABILITY

Lead contact

Further information and requests for resources and reagents should be directed to and will be fulfilled by the Lead Contact, Benjamin Tu (benjamin.tu@utsouthwestern.edu).

Materials availability

Reagents are available upon request from the Lead Contact.

Data and code availability

All sequencing data have been deposited in Gene Expression Omnibus with the accession number GEO: GSE142528.

EXPERIMENTAL MODEL AND SUBJECT DETAILS

Yeast strains and growth conditions

Prototrophic CEN.PK *Saccharomyces cerevisiae* ([van Dijken et al., 2000](#)) was used for strain construction ([Table S4](#)), using the lithium acetate based transformation protocol ([Longtine et al., 1998](#)). Unless otherwise stated, yeast strains were grown in SD medium containing 20 g L⁻¹ glucose and 6.7 g L⁻¹ yeast nitrogen base without amino acids (BD Difco) at 30°C and 300 rpm. For nutrient starvation experiments, medium formulas are listed in [Table S5](#). Plasmids were constructed using the Gibson assembly protocol ([Gibson et al., 2009](#)) and site directed mutagenesis was performed using Phusion HF polymerase (NEB) with primers bearing the desired mutations ([Table S4](#)), followed by DpnI (NEB) digestion and subsequent transformation into *E. coli* DH5 α . All the plasmids were verified by DNA sequencing.

Mammalian cell lines and growth conditions

All cell lines (HeLa, HEK293T, and 3T3, see [Key resources table](#) for details) were cultured in a Heracell humidified incubator (Thermo-fisher, HERAcCell 150i) at 37°C with 5% CO₂. HeLa cells were maintained in RPMI-1640 (GIBCO A14517-01), and 3T3 and HEK293T cells in DMEM (GIBCO 21013-024). Both media were supplemented with the required amino acids and 5% fetal bovine serum (Sigma F6178). When confluency reached ~80%, cells were washed with PBS twice and subsequently cultured in either RPMI-1640 (GIBCO A14517-01) or DMEM (GIBCO 21013-024) with or without methionine. After six hours, cells were harvested and total RNA was isolated using the TRIzol reagent (Invitrogen, Thermo Fisher), as described below.

METHOD DETAILS

Total RNA isolation

Yeast cell pellet stored at -80°C was thawed on ice and washed with ice-cold sterile water once. TES (10 mM Tris-HCl pH 7.5, 10 mM EDTA pH 8.0, and 0.5% SDS) was added to resuspend the cell pellet followed by addition of an equal volume of acidic phenol (pH 4.3). Cells were lysed using acid-washed glass beads on a bead beater (two cycles of one-minute beating followed by one-minute cooling on ice). Cell debris and glass beads were removed by centrifugation. The aqueous phase was transferred into a clean centrifuge tube and extracted with an equal volume of acidic phenol, followed by a third extraction with chloroform to remove the residual phenol. RNA was ethanol precipitated, washed with 70% ethanol, and dried before finally being dissolved in nuclease-free water. Purified RNA was examined electrophoretically and quantified spectrophotometrically.

Mammalian RNA was isolated using the TRIzol reagent (Invitrogen, Thermo Fisher). Briefly, 2 mL TRIzol was dispensed into 15-cm dish and cell suspension was collected by pipetting. Cell pellet was either stored at -80°C or processed immediately. To 1 mL TRIzol cell suspension, 250 μ L chloroform was added. The mixture was vortexed vigorously and centrifuged. The aqueous phase was transferred to a clean centrifuge tube with 600 μ L isopropanol and precipitated on ice. RNA was pelleted by centrifugation and washed with 70% ethanol once to remove salts. RNA was then resuspended in nuclease-free water and digested with DNase I to remove

DNA. DNase I was subsequently removed using phenol (pH 4.3):chloroform (1:1) extraction and RNA was recovered by ethanol precipitation. RNA was washed once with 70% ethanol and resuspended in nuclease-free water.

RNA fractionation

Small RNA was purified using the PureLink miRNA isolation kit (Invitrogen) and polyA⁺ RNA was isolated using the Dynabeads mRNA purification kit (Invitrogen) following the manufacturers' instructions. To isolate 18S and 25S rRNA, we mixed total RNA with an equal volume of 2 × RNA loading solution (95% formamide, 0.02% SDS, 0.02% bromophenol blue, and 1 mM EDTA pH 8.0) and denatured RNA samples at 75°C for five minutes followed by rapid chilling on ice. Denatured RNA was loaded onto a 1.3% TAE low melting agarose gel. The 18S and 25S rRNA were visualized by ethidium bromide staining, excised using a clean scalpel, and purified using the NucleoSpin Gel and PCR clean-up kit (Takara) following the manufacturer's instructions.

Estimation of stoichiometry of m⁶A in yeast 18S rRNA

We used HeLa 18S rRNA as the standard, since it is modified with a single m⁶A at A1832 to ~98% (Liu et al., 2013). Yeast and HeLa 18S rRNA were digested and ribonucleosides were quantified as described below. The abundance of m⁶A was normalized to each of the four ribonucleosides (A, G, C, and U). These ratios were further corrected to account for the differences in the abundance of each ribonucleoside between yeast and HeLa cells. The stoichiometry of m⁶A in yeast 18S rRNA was then estimated by comparing the normalized m⁶A (e.g., m⁶A/A) between yeast and HeLa cells. Normalization by each of the four ribonucleosides gave similar results, averaging between 4%–5% of m⁶A per 18S rRNA.

Mung bean nuclease (MBN) protection assay

This assay was performed as described previously (Andersen et al., 2004; Peifer et al., 2013; Sharma et al., 2013) with some modifications. A total of ~1000 pmole DNA oligo was mixed with 200 μg total RNA. After ethanol precipitation and wash, the nucleic acid mixture was resuspended in 40 μL 1 × hybridization buffer (40 mM PIPES pH 6.4, 400 mM NaCl, 1 mM EDTA, and 20% formamide) and heated at 85°C for ten minutes followed by incubation at 35°C for three hours. The hybridization mixture was then mixed with 497 μL nuclease-free water, 60 μL 10 × RNA digestion buffer (100 mM Tris-HCl pH 7.5, 3 M sodium acetate pH 5.2, 50 mM EDTA pH 8.0), and 3 μL 5 mg ml⁻¹ RNase A (Epicenter), and incubated at 37°C for one hour. The digestion mixture was then extracted with an equal volume of acidic phenol (pH 4.3):chloroform (1:1) and ethanol precipitated. The nucleic acid pellet was washed, resuspended in 100 μL 1 × MBN buffer (30 mM NaCl, 50 mM sodium acetate, 1 mM ZnSO₄, pH 5.0) supplemented with 4.5 μL 10 U μl⁻¹ MBN (NEB), and incubated at 30°C for one hour. The digestion mixture was then extracted with an equal volume of acidic phenol (pH 4.3): chloroform (1:1) and ethanol precipitated. The precipitated nucleic acid was loaded onto a 15% polyacrylamide gel and the RNA:DNA hybrid was visualized by ethidium bromide staining and excised using a clean scalpel. The gel slice was transferred to a clean microcentrifuge tube, crushed, and soaked in 200 μL elution buffer containing 300 mM sodium acetate (pH 5.3), 1 mM EDTA (pH 8.0), and 0.1% SDS. The eluted RNA:DNA fragment was ethanol precipitated, washed, and resuspended in nuclease-free water. Alternatively, the RNA:DNA hybrid was extracted using D-Tube Dialyzer Mini (MWCO 6-8 kDa) (EMD Millipore) by electro-elution following the manufacturer's instructions.

LC-MS/MS detection of nucleosides

RNA digestion and nucleoside detection were performed essentially as described by Laxman et al. (2013). Briefly, RNA was resuspended in 102 μL of ultrapure water and 7 μL of acidic buffer (0.1 M sodium acetate, 20 mM ZnCl₂, pH 6.8) was added, followed by the addition of 5 μg RNase A (Epicenter) and 1.5 U nuclease P1 (Sigma). Digestion was carried out at 37°C for four hours before 7 μL of basic buffer (0.3 M sodium acetate, pH 7.8) was added. The digestion mixture was further treated with 10 U alkaline phosphatase (calf intestinal, NEB) and 5 μL 8 mg ml⁻¹ snake venom phosphodiesterase I (Sigma) overnight to maximize digestion and dephosphorylation efficiency.

The digested samples were separated on a Synergi Fusion-RP column (4 μm particle size, 80 Å pore size, 150 mm × 2 mm, Phenomenex) using a Shimadzu high performance liquid chromatography (HPLC) machine and simultaneously detected under positive mode by a triple quadrupole mass spectrometer (3200 QTRAP, ABSCIEX). The total run time was 25 minutes at a flow rate of 0.5 mL min⁻¹, with 5 mM ammonium acetate (pH 5.5) in water as solvent A and 5 mM ammonium acetate in methanol as solvent B. The following gradient elution was performed: 0.01 min, 0% B, 4 min, 0% B, 5 min, 0.2% B, 6 min, 1% B, 7 min, 3% B, 8 min, 5% B, 14 min, 25% B, 16 min, 50% B, 18 min, 100% B, 22 min, 100% B, 23 min, 0% B, 25 min, 0% B. Ribonucleosides were quantified using the Analyst software package 1.6.2 or 1.6.3 by calculating the total peak area. For each experiment, authentic standards were injected and analyzed alongside samples.

LC-MS/MS detection of metabolites

The extraction protocol comprised two sequential steps: quenching and extraction, as described in Castrillo et al. (2003) and Gonzalez et al. (1997), respectively. To quench cells, one volume of cell culture was mixed with three volumes of methanol-water solution (60% v/v, buffered with 10 mM Tricine to pH 7.4) kept at -40°C. Quenched cells were centrifuged and resuspended in extraction buffer containing ethanol-water solution (75% v/v, 0.1% formic acid to minimize oxidation of thiols) and heated at 80°C for three

minutes. Cell extraction was immediately chilled on ice and subsequently centrifuged at maximum speed at 0°C to remove cell debris. The supernatant was vacuum dried and stored at –80°C until analysis.

Samples were analyzed using reversed-phase HPLC coupled to tandem mass spectrometry as described previously (Tu et al., 2007). Metabolites were separated on a Synergi Fusion-RP column (4 μm particle size, 80 Å pore size, 150 mm × 2 mm, Phenomenex) using a Shimadzu HPLC machine and simultaneously detected by a triple quadrupole mass spectrometer (3200 QTRAP, AB SCIEX). The total run time was 22 minutes at a flow rate of 0.5 mL min⁻¹, with 0.1% (v/v) formic acid in water as solvent A and 0.1% (v/v) formic acid in methanol as solvent B. The following gradient elution was performed: 0.01 min, 0% B, 4 min, 0% B, 11 min, 50% B, 13 min, 100% B, 17 min, 100% B, 18 min, 0% B, 22 min, 0% B. Metabolites were detected by multiple reaction monitoring (MRM) with transitions listed in Table S6. Metabolites were quantified using the Analyst software package 1.6.2 or 1.6.3 by calculating total peak area.

Competition assay

Competition between various strains was performed as described previously (Sankar et al., 2016), with some modifications. To distinguish between *dim1* and WT, the *E. coli lacZ* gene controlled by the *TEF1* promoter and *CYC1* terminator was inserted into an intergenic region between *NCA3* and *ASF1*. This site was selected according to Mikkelsen et al. (2012), who reported that a similar integration in this region supports robust *lacZ* expression and does not noticeably impact growth. To control for the impact of *lacZ* expression on fitness, the *lacZ* cassette was integrated into both *dim1* mutants and WT. For example, for competition between WT and the E85Q mutant, two experiments (*a* and *b*) were performed in parallel with the following combinations: WT-*lacZ* versus E85Q and WT versus E85Q-*lacZ*. Cells were first acclimated in complete medium and then grown in fresh complete medium to log phase. To start the competition, two competitors were mixed at a ratio of 1:1, with each having an initial OD₆₀₀ ~0.01. Cells were grown to saturation (~7-8 doublings) and were diluted into fresh complete medium in 1:200 after approximately 24 hours. This was then repeated for a minimum of four times and the first round of competition was typically excluded for fitness calculation as cells were just beginning to adapt to the new environment. Nevertheless, cells were plated onto synthetic defined agar plates (6.7 g L⁻¹ yeast nitrogen base without amino acids (BD Difco), 0.79 g L⁻¹ CSM (Sunrise Science), 20 g L⁻¹ glucose, and 20 g L⁻¹ agar), supplemented with 80 μg mL⁻¹ 5-bromo-4-chloro-3-indolyl-β-D-galactopyranoside (X-gal) and BU salts (26.1 mM Na₂HPO₄ and 25 mM NaH₂PO₄, pH 7.0). Blue (competitor expressing *lacZ*) and white colonies were counted in duplicate to minimize counting errors. Fitness was calculated relative to WT using the following equations:

$$f_a^i = \frac{T_{dim1-lacZ}^i}{T_{DIM1}^i}$$

$$f_b^i = \frac{T_{dim1}^i}{T_{DIM1-lacZ}^i}$$

$$\bar{f}_a = \frac{1}{n} \sum_1^n f_a^i$$

$$\bar{f}_b = \frac{1}{n} \sum_1^n f_b^i$$

$$\bar{f} = \sqrt{\bar{f}_a \times \bar{f}_b}$$

, where f_a^i and f_b^i are the relative fitness of *dim1-lacZ* to WT and *dim1* to WT-*lacZ* in the *i*th round of competition, respectively; $T_{genotype}^i$ is the number of doublings of a particular strain during a 24-hour competition and *i* is the *i*th round of competition; \bar{f}_a and \bar{f}_b are the arithmetic mean fitness of *dim1-lacZ* to WT and *dim1* to WT-*lacZ*, respectively. \bar{f} is the geometric mean fitness of *dim1* relative to WT, which was reported in Figure 3E.

Dual-luciferase assay

The dual-luciferase assay was performed as described previously (Ghalei et al., 2017; Salas-Marco and Bedwell, 2005), using the Dual Luciferase Reporter Assay System (Promega) with some modifications. When cells reached log phase, one mL of culture was collected by centrifugation and cell pellets were snap frozen in liquid nitrogen and stored at –80°C until analysis. Cell pellets were first thawed on ice and washed once with ice-cold water to remove the residual medium. Cells were then lysed in 100 μL passive

lysis buffer at room temperature for one minute and 10 μL was added to 30 μL Luciferase Assay Reagent II to measure Firefly luciferase activity, followed by the addition of 30 μL Stop & Glow Reagent to measure Renilla luciferase activity. Luminescence was recorded for ten seconds in a 96-well flat-bottom black polystyrene plate (COSTAR) on a Synergy 2 plate reader (BioTek) at room temperature and reported in relative luminescence units (RLU). Background-subtracted Firefly luciferase activity was subsequently normalized to background-subtracted Renilla luciferase activity.

Polysome profiling

Samples for polysome profiling were prepared as described with some modifications (Mašek et al., 2011). When cells were ready, cycloheximide (dissolved in 100% ethanol) was added to a final concentration of 0.1 mg mL^{-1} and frozen ice at -20°C (2 g per 10 mL culture) was added to rapidly chill cells. After further incubation on ice for five minutes, cells were centrifuged at 4°C , snap frozen in liquid nitrogen, and stored at -80°C until processing. Frozen cell pellets were thawed on ice and washed twice in polysome extraction buffer (PEB) (20 mM Tris-HCl pH 7.5, 140 mM KCl, 5 mM MgCl_2 , 0.1 mg mL^{-1} cycloheximide, 1% Triton X-100, and 0.5 mM DTT). Cells were subsequently lysed in PEB with glass beads on a bead beater following three rounds of beating (30 s beating and two-minute cooling on ice). Cell debris was removed by centrifugation at $8000 \times g$ for five minutes at 4°C and supernatant was collected and measured spectrophotometrically at 260 nm. A 10%–50% (w/v) sucrose gradient was prepared using BIOCAMP Gradient Station *ip* in 20 mM Tris-HCl pH 7.5, 140 mM KCl, 5 mM MgCl_2 , 0.1 mg mL^{-1} cycloheximide, and 0.5 mM DTT. Approximately one A_{260} unit of cell lysates was carefully loaded onto the top of the sucrose gradient and centrifuged at $41,000 \times g$ for two hours at 4°C . Polysome profiles were recorded using BIOCAMP Gradient Station *ip* by measuring absorbance at 260 nm.

Western blot

Samples for western blot were quenched in 10% trichloroacetic acid (TCA) for ten minutes on ice and then stored at -80°C until analysis. Cell pellets were washed once in cold acetone to remove the residual TCA, before bead-beating in urea lysis buffer containing 6 M urea, 1% SDS, 50 mM Tris-HCl (pH 7.5), 5 mM EDTA, 1 mM DTT, 1 mM PMSF, 10 μM leupeptin, 5 mM pepstatin A, and 1 \times protease inhibitor cocktail (Roche). Lysates were heated for five minutes at 75°C and then centrifuged at maximum speed for five minutes. Protein concentration was estimated using the bicinchoninic acid assay (Thermo Fisher Scientific) and equal amounts of proteins were separated by electrophoresis using 4%–12% NuPAGE gels. Proteins were then transferred to a nitrocellulose membrane and blotted with the corresponding antibodies. Blocking was performed in 5% dry milk/TBST, while antibody incubation was in 1% dry milk/TBST. Antibodies were used at the following dilutions: α -FLAG 1:3,000 (Sigma F1804), α -Rpn10p 1:40,000 (Abcam ab98843), α -G6pdhp 1:20,000 (Sigma A9521).

Northern blot

Northern blot was performed as described previously (Josefsen and Nielsen, 2011; Tafforeau et al., 2013), with minor modifications. Briefly, total RNA of equal amounts was separated on a 1.2% denaturing formaldehyde agarose gel and transferred to a nylon membrane (Hybond- N^+ , GE healthcare). RNA was crosslinked to the membrane using a UV-cross linker (Stratagene) and stained with methylene blue (0.02% in 0.3 M sodium acetate, pH 5.0). Membrane was washed in nuclease-free water a few times to remove the dye and images were taken using the ChemiDoc MP Imaging System (Bio-Rad). Membrane was pre-hybridized in hybridization solution containing 50% deionized formamide, 5 \times SSPE, 5 \times Denhardt's solution, and 1% SDS at 65°C for one hour. The hybridization solution was discarded and fresh solution with 10 pM biotinylated DNA probe was added. Membrane was incubated at 65°C for another hour and then at 37°C overnight. Membrane-bound biotinylated DNA probes were detected using the Chemiluminescent Nucleic Acid Detection Module (Thermo Fisher) following the manufacturer's recommendations. Images were taken using the ChemiDoc MP Imaging System and processed using Image Lab 6.0 (Bio-Rad). Biotinylated DNA probes were stripped from the membrane in 50% deionized formamide and 2 \times SSPE at 65°C for one hour to allow for subsequent hybridization.

Ribosome profiling

Yeast cells were grown in sulfur free (see formula in Table S5) + 1 mM methionine (SFM) to saturation and diluted into 20 mL SFM with a starting $\text{OD}_{600} \sim 0.1$. Cells were grown to log phase and diluted into 320 mL SFM with a starting $\text{OD}_{600} \sim 0.005$. When OD_{600} reached ~ 0.5 – 0.6 , cells were harvested according to Santos et al. (2019). Briefly, 200 mL pre-starvation culture was transferred into a pre-warmed (30°C) vacuum filtration apparatus and cells were collected onto a 0.45 μm cellulose nitrate membrane filter (Whatman). Before the medium was completely drained, cell pellet was rapidly scraped using a clean metal spatula and transferred into liquid nitrogen. The remaining culture was spun down at $4000 \times g$ for one minute and washed once with an equal volume pre-warmed (30°C) SF medium once. Washed cells were resuspended in an equal volume pre-warmed (30°C) SF. After two hours, cells were collected exactly as described above and cell pellets were stored at -80°C until analysis.

Frozen cell pellets were cryogenically pulverized on a SPEX 6870 Freezer/Mill for one minute at 15 cycles per minute and frozen droplets of lysis buffer (20 mM Tris-HCl pH 8.0, 140 mM KCl, 5 mM MgCl_2 , 1 mM dithiothreitol, 100 $\mu\text{g mL}^{-1}$ cycloheximide, 1% Triton X-100, and 0.025 U μL^{-1} Turbo DNase) were added. The cell lysate was thawed, and cell debris was removed by two sequential centrifugation steps at 4°C : first at $3000 \times g$ for five minutes and then at $20,000 \times g$ for ten minutes.

Libraries for ribosome profiling and RNA-seq were constructed essentially as described by McGlincy and Ingolia (2017). Briefly, ribosome-protected RNA fragments ranging from ~ 15 – 34 nt were isolated after RNase I digestion and denaturing PAGE separation.

Cloning linkers with 3' barcode sequences were ligated to RNA footprints and samples of unique barcodes were pooled together post-ligation whenever possible. rRNA was depleted sequentially using Ribo-Zero Gold for Yeast (Illumina) and biotinylated anti-sense oligos against rRNA species that co-migrate with ribosome footprints as described by Brar et al. (2012). For RNA-seq, RNA was extracted from the clarified lysates using TRIzol (Invitrogen) and rRNA was depleted using Ribo-Zero Gold for Yeast (Illumina). The processed RNA was then used to generate TruSeq Stranded libraries (Illumina) following the manufacturer's recommendations. Libraries of ribosome profiling and RNA-seq were sequenced on an Illumina HiSeq 4000 in single read 50-base mode. Each set of matched ribosome profiling and RNA-seq data are derived from a single biological sample (two biological replicates in total for each strain under each condition).

Sequencing data analysis

FASTX-clipper and -barcode splitter (http://hannonlab.cshl.edu/fastx_toolkit/) were used to remove the linker sequences and demultiplex ribosome profiling data, respectively. Unique molecular identifiers and sample barcodes were subsequently removed using a custom Python script. Reads corresponding to rRNAs and tRNAs were excluded using Bowtie v1.1.2 (<http://bowtie-bio.sourceforge.net/>) and the remaining reads were aligned to *Saccharomyces cerevisiae* genome using tophat v2.1.1 (<https://ccb.jhu.edu/software/tophat/>). We then used the plastid cs program (Dunn and Weissman, 2016) to calculate counts per gene and normalized counts per gene (in reads per kilobase per million mapped reads, or RPKM), with counts assigned to the ribosome P-site determined by the plastid *psite* program. Genome regions that could not be uniquely mapped from a 26-base read with two mismatches were identified by the plastid *crossmap* program, which, together with the first 30 and last five codons of each coding sequence (CDS), were excluded from count assignments and RPKM calculations. RNA-seq data were analyzed similarly. However, because of the TruSeq Stranded chemistry, the reads had to be reverse-complemented prior to plastid analysis, and counts were assigned to the 5'-most aligned base. We used the plastid *make wiggle* program to generate Wiggle files from genome alignments for subsequent data visualization in the IGV browser (<http://software.broadinstitute.org/software/igv/>). For visualization purposes, Wiggle counts were assigned to the ribosome P-site for ribosome profiling, or equally apportioned across reads for RNA-seq. Dubious ORFs listed in the *Saccharomyces* Genome Database (SGD, <https://www.yeastgenome.org/>) were not considered for analysis.

Translation efficiency (TE) is defined as the ratio of normalized ribosome footprint counts to normalized mRNA counts. TE and mRNA fold changes and adjusted p values were calculated from raw counts with DESeq2 (Love et al., 2014). TE changes were calculated using the design formula \sim sample + sample:assay, where the sample interaction term denotes the growth condition and genotype (e.g., SFM_E85Q) and the assay interaction term specifies whether counts are derived from RNA-seq or ribosome profiling. mRNA changes were calculated from RNA-seq counts using the design formula \sim sample.

Metacodon analysis

Ribosome profiling data were processed to produce mean relative enrichment values for each codon as described in Hussmann et al. (2015). Briefly, footprint sequencing reads were trimmed of adaptor sequence, aligned to the yeast genome and spliced transcriptome with TopHat2 (Kim et al., 2013), and assigned to the codon positioned in the A-site of the footprint as in Ingolia et al. (2009). For each gene, the raw counts of uniquely mapped footprints with their A-site over each codon were normalized by dividing by the average count for all codons in that gene to produce a relative enrichment value for each codon. The mean relative enrichment for each codon type was then calculated by averaging the relative enrichment value at every occurrence of that codon type located at least 90 codons away from the start or stop codon of its gene. To reduce noise, genes with less than 0.1 mean footprints per codon were excluded from averaging.

QUANTIFICATION AND STATISTICAL ANALYSIS

All statistical analyses were performed in GraphPad Prism (versions 6, 7, 8, and 9), with details provided in the corresponding figure legends, such as statistical tests employed, values and definition of n, and definition of center and dispersion. No methods were used to determine whether the data met assumptions of the statistical approach.

Cell Reports, Volume 34

Supplemental information

Regulation of translation

by methylation multiplicity of 18S rRNA

Kuanqing Liu, Daniel A. Santos, Jeffrey A. Hussmann, Yun Wang, Benjamin M. Sutter, Jonathan S. Weissman, and Benjamin P. Tu

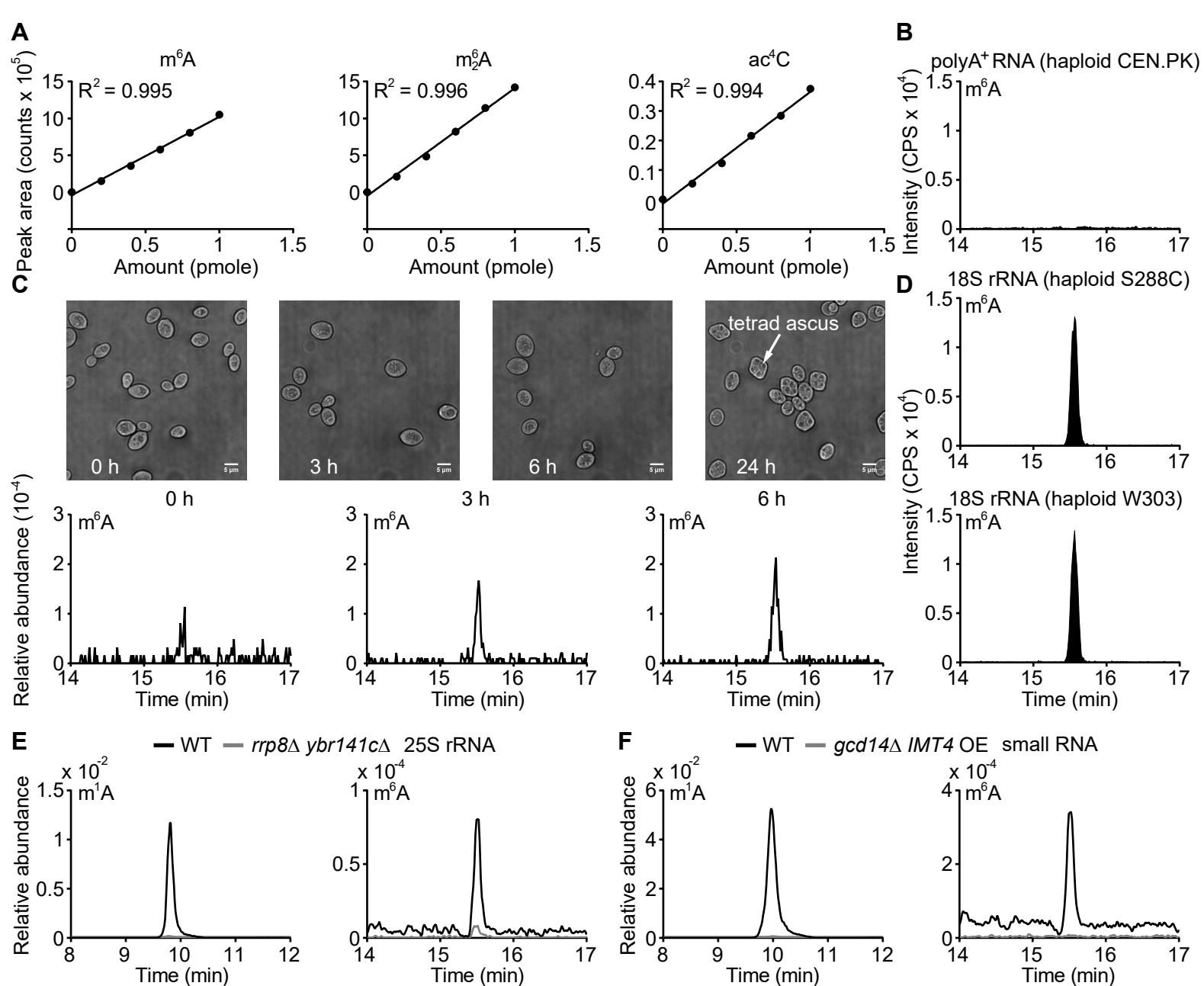


Figure S1. Detection of m^6A in 18S rRNA from vegetatively growing haploid yeast cells. Related to Figure 1.

(A) Standard curves for m^6A , m^6_2A , and ac^4C . (B) m^6A is not detected in polyA⁺ RNA from vegetatively growing haploid yeast (CEN.PK). (C) m^6A levels in polyA⁺ RNA increase during sporulation. KL139 (CEN.PK diploid) was induced to sporulate as described exactly by Agarwala et al. (Agarwala et al. 2012). Samples were collected, immediately (0 h), three (3 h), and six hours (6 h) after cells were resuspended in sporulation medium (0.3% potassium acetate). Total RNA was isolated as described in STAR METHODS and polyA⁺ RNA was purified from total RNA using the Dynabeads mRNA kit (Invitrogen). Approximately 1 μ g polyA⁺ RNA was digested and analyzed by LC-MS/MS. Each chromatogram was normalized by the abundance of adenosine to allow for comparison between time points. Scale bar = 5 μ m. (D) m^6A is detected in 18S rRNA isolated from vegetatively growing haploid yeast cells (strains: S288C and W303). m^6A detected in 25S (E) and small RNA (F) is likely derived from m^1A via Dimroth rearrangement. OE: overexpression. m^1A and m^6A can be detected by the same MRM transition (282/150), but are eluted at different times. Each chromatogram was normalized by the abundance of adenosine to allow for comparison between different conditions. The essential tRNA m^1A methyltransferase Gcd14p becomes dispensable when the initiator methionyl tRNA gene *IMT4* is overexpressed (Calvo O, et al. 1999).

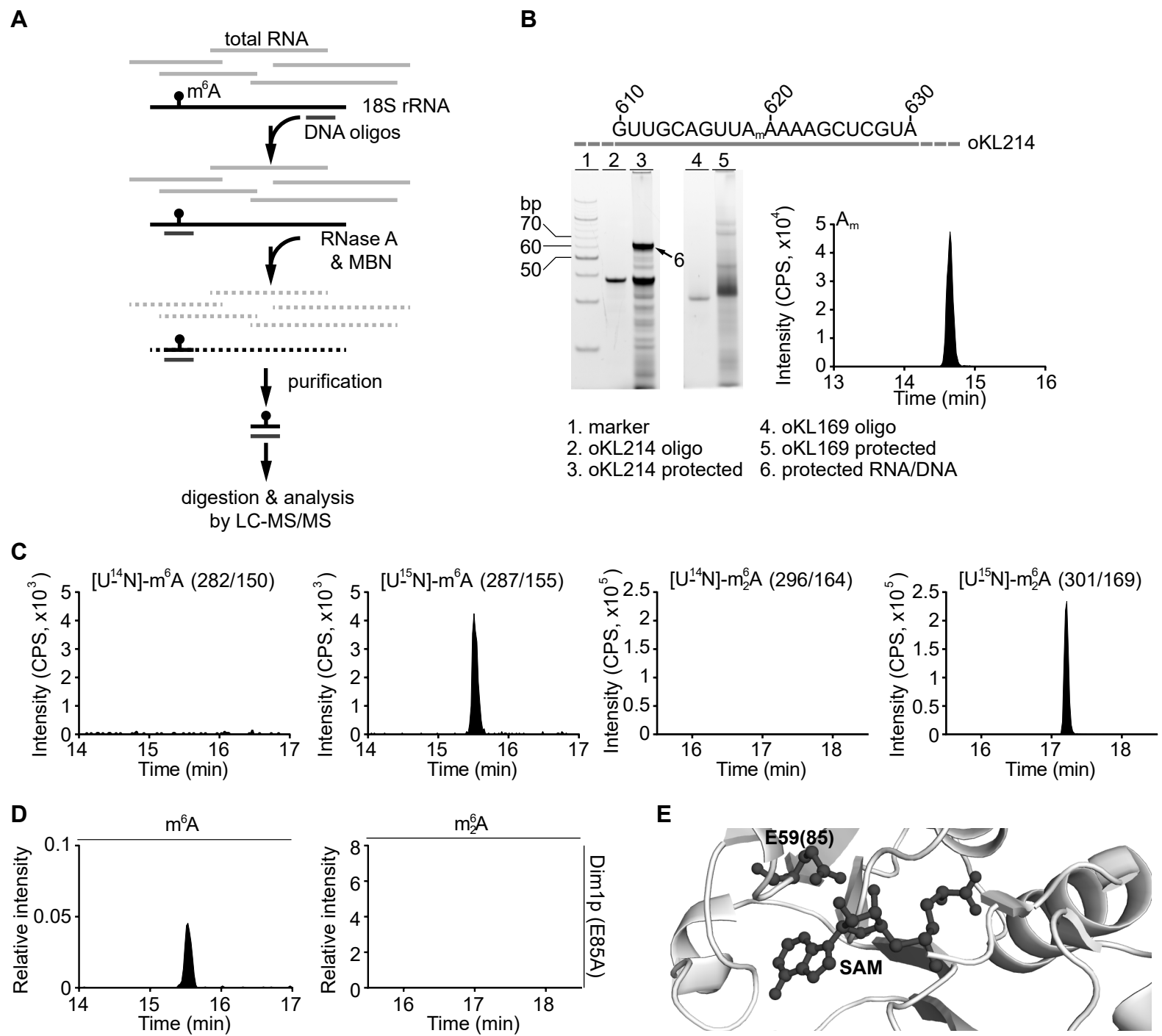


Figure S2. Validation of m^6A in yeast 18S rRNA. Related to Figure 1.

(A) Schematic of the mung bean nuclease (MBN) protection assay. **(B)** Detection of the expected 2'-O-methyladenosine (A_m) at 619 in 18S rRNA. oKL169 is not complementary to any yeast RNA and thus did not yield a RNA/DNA hybrid after digestion by RNase A and MBN. **(C)** m^6A and m^2A are derived from growing yeast cells, not from contamination during sample processing. WT cells were grown from a single colony in $[^{15}N]$ SD (1.7 g L⁻¹ yeast nitrogen base without ammonium sulfate and amino acids (BD Difco), 2% glucose, and 5 g L⁻¹ (^{15}NH)₂SO₄ (ISOTEC). Cells were diluted in the same medium with a starting OD₆₀₀ ~0.01 and grown to saturation. Cells were then diluted in the same medium with a starting OD₆₀₀ ~0.1 and grown to log phase before harvest. Total RNA was isolated and the 3' fragment of 18S rRNA was isolated using the MBN protection assay with oKL204 and analyzed by LC-MS/MS. **(D)** The Dim1p (E85A) mutant is still able to synthesize m^6A , but not m^2A . **(E)** Active site of *Methanocaldococcus jannaschii* Dim1. The structure was adapted from PDB#3GRY (O'Farrell et al. 2010) and prepared using Pymol (<https://pymol.org>). The number in parentheses corresponds to the position in *S. cerevisiae* Dim1p.

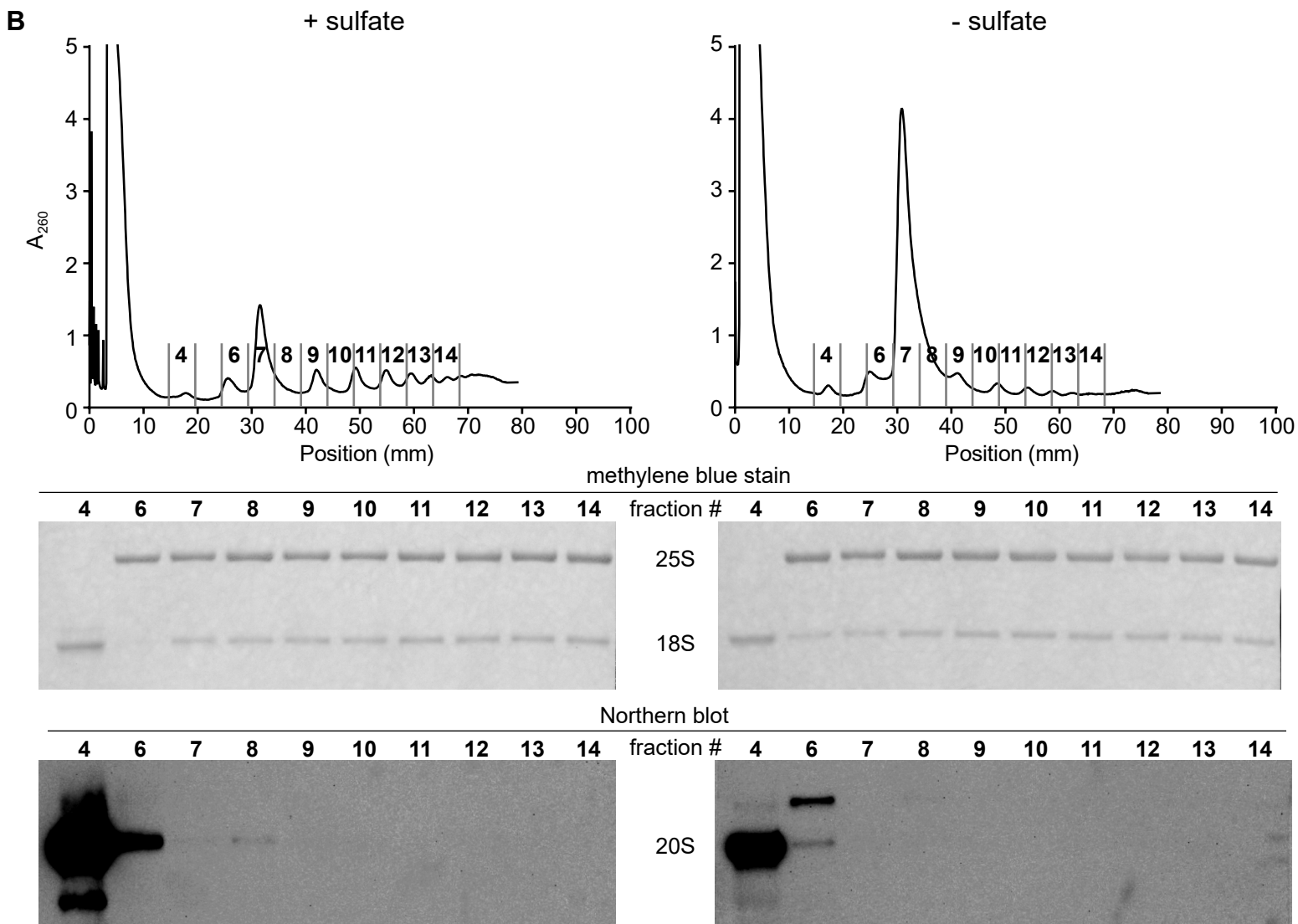
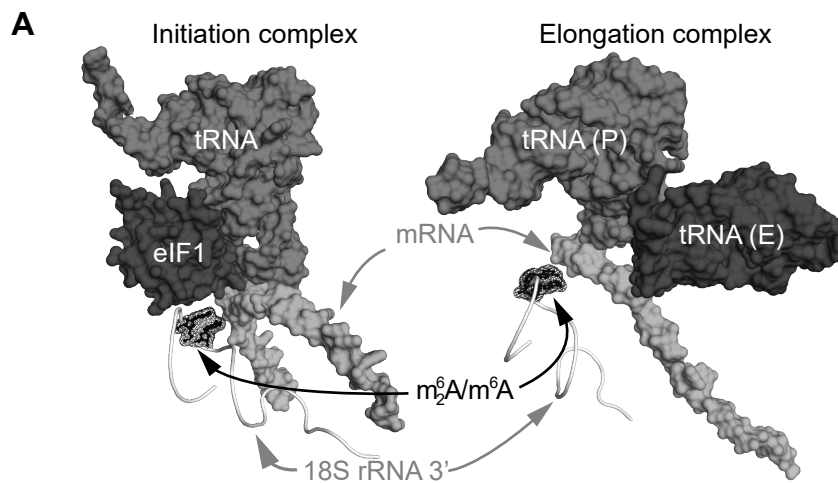


Figure S4. m^6A -bearing ribosomes engage in active translation. Related to Figure 3.

(A) m^6A/m^2A resides close to the ribosome P-site. Structures of initiation and elongation complexes were adapted from PDB#3J81 (Hussain et al. 2014), and PDB#6Q8Y (Tesina et al. 2019), respectively, and prepared using Pymol (<https://pymol.org>). tRNA (P) and tRNA (E) occupy the P- and E-sites of the ribosome, respectively. (B) 20S rRNA is absent from polysome fractions under sulfate-replete and -starvation conditions. Cells were grown in complete medium to log phase and starved of sulfate for two hours. Samples were collected for polysome profiling as described in STAR METHODS. Sucrose fractions were extracted with an equal volume of phenol (pH 4.3)/chloroform and nucleic acids were precipitated with an equal volume of isopropanol. Northern blot was performed as described in STAR METHODS.

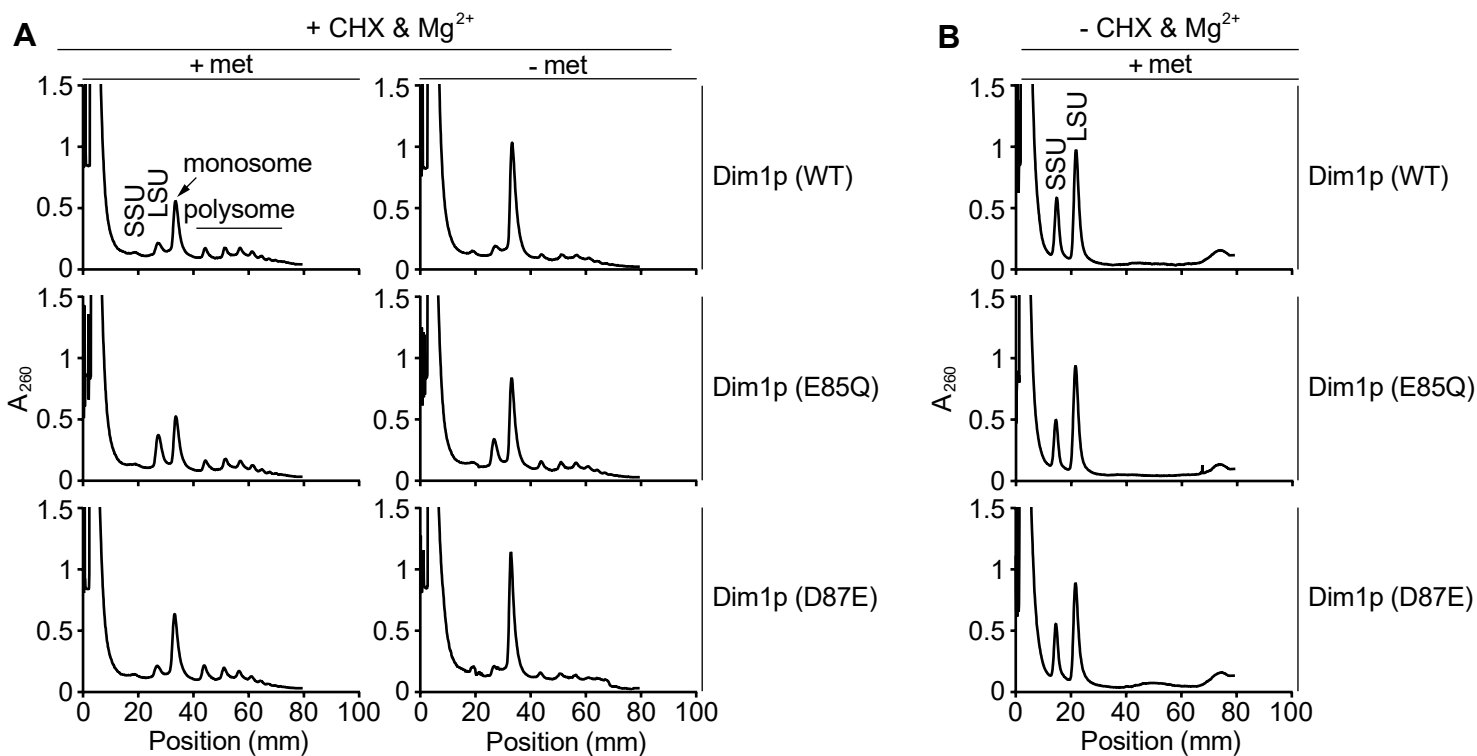


Figure S5. Analysis of ribosome biogenesis in *dim1* mutants. Related to Figure 4.

(A) Polysome profiling. SSU: small subunit (40S); LSU: large subunit (60S). Cells were grown in SFM and starved of methionine in SF for 2 h. Samples were collected for polysome profiling as described in STAR METHODS. **(B)** Ribosome subunit profiling. Cells were grown in SFM and collected without cycloheximide (CHX), and were lysed in the absence of magnesium to separate the two subunits.

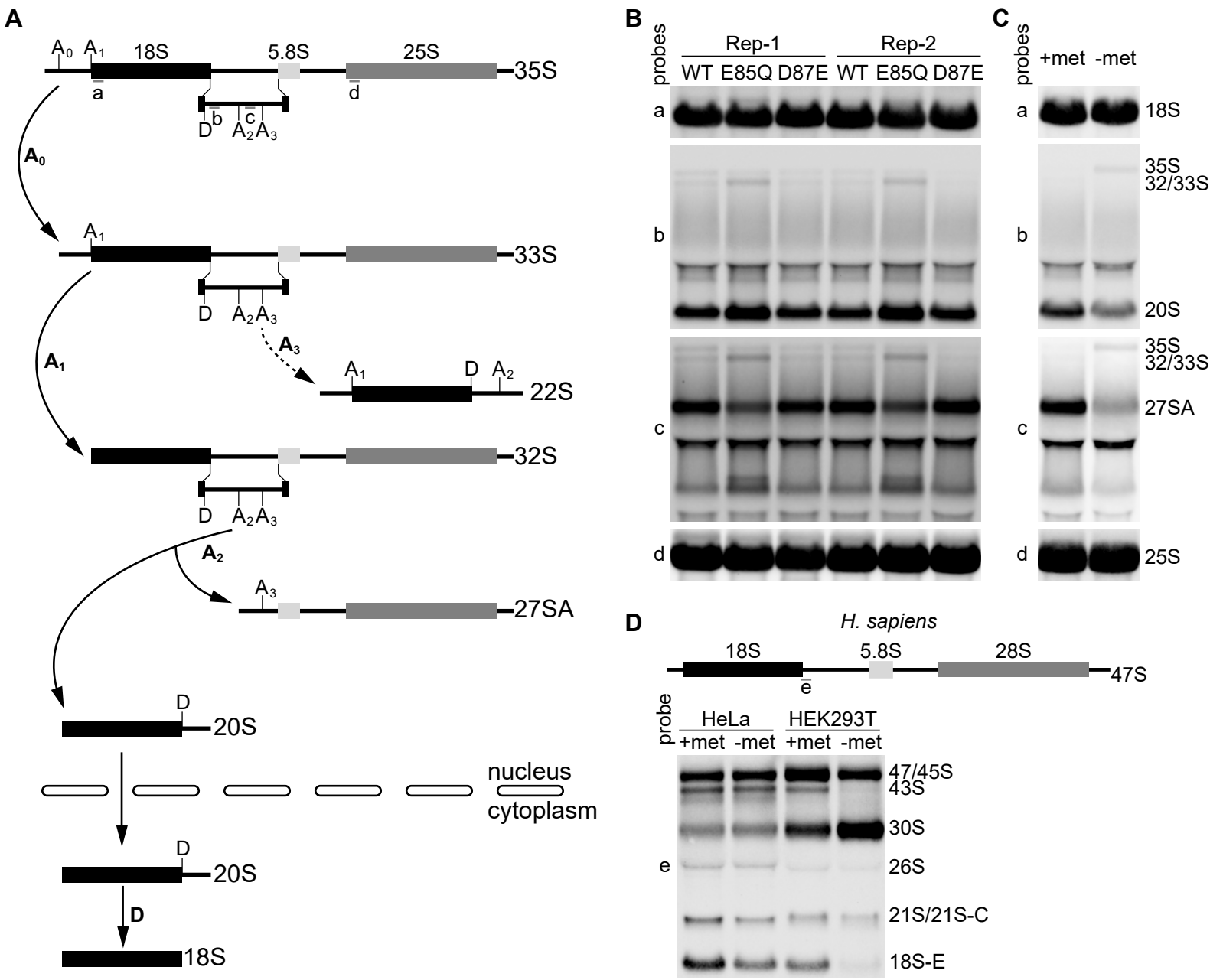
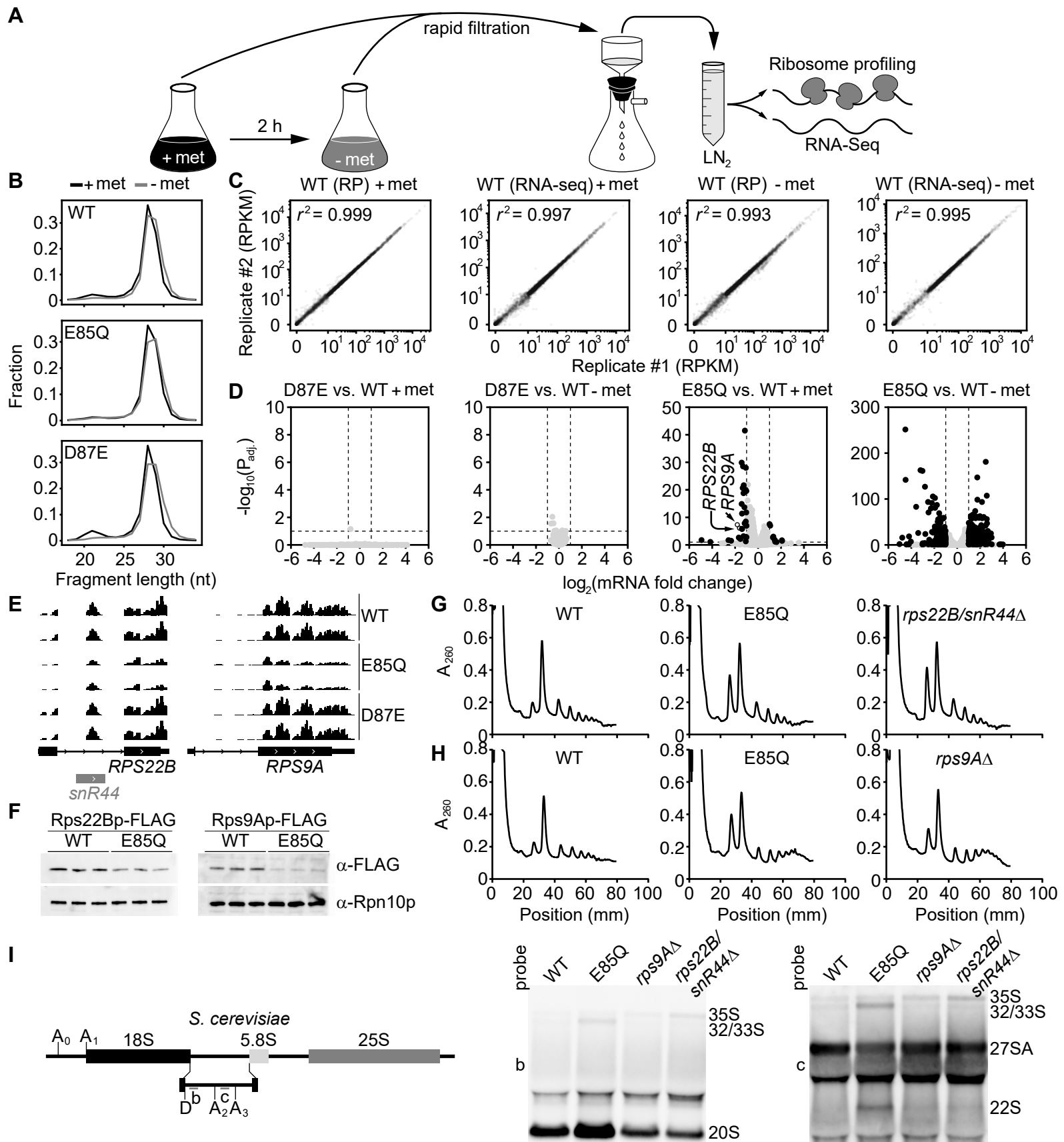


Figure S6. Analysis of rRNA processing in yeast and human cell lines. Related to Figure 4.
(A) Simplified schematic of rRNA processing in yeast. Only relevant processing intermediates and cleavage sites were shown. Probes used for Northern blot were also indicated. The 22S pre-rRNA is thought to arise from cleavage at A3 of the 33S pre-rRNA, observed when Dim1p is depleted (Lafontaine et al., 1995). **(B)** The E85Q mutation, but not the D87E mutation causes rRNA processing defects. **(C)** Examination of rRNA processing in WT yeast cells grown with methionine and without methionine (2 h) using Northern blot. **(D)** Examination of rRNA processing in mammalian cell lines grown with and without methionine (6 h) using Northern blot.



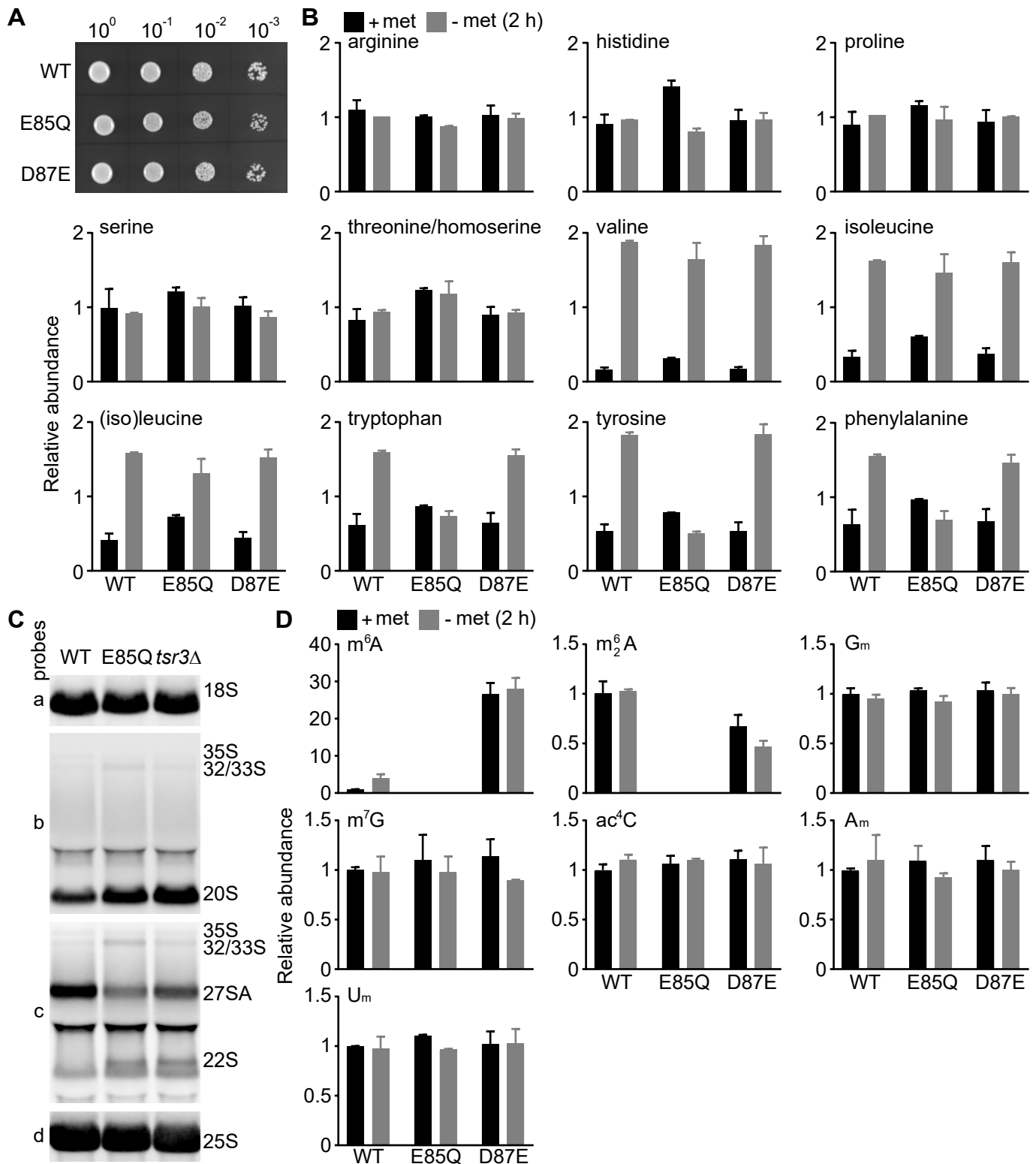
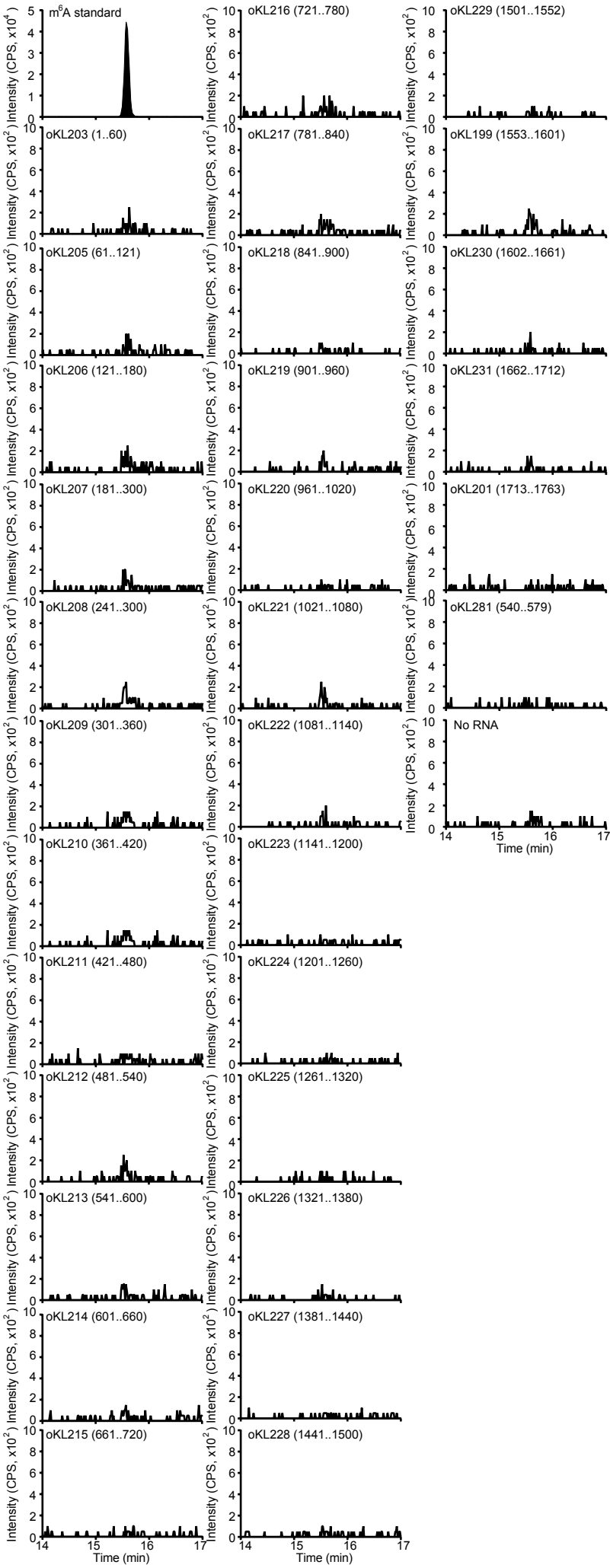
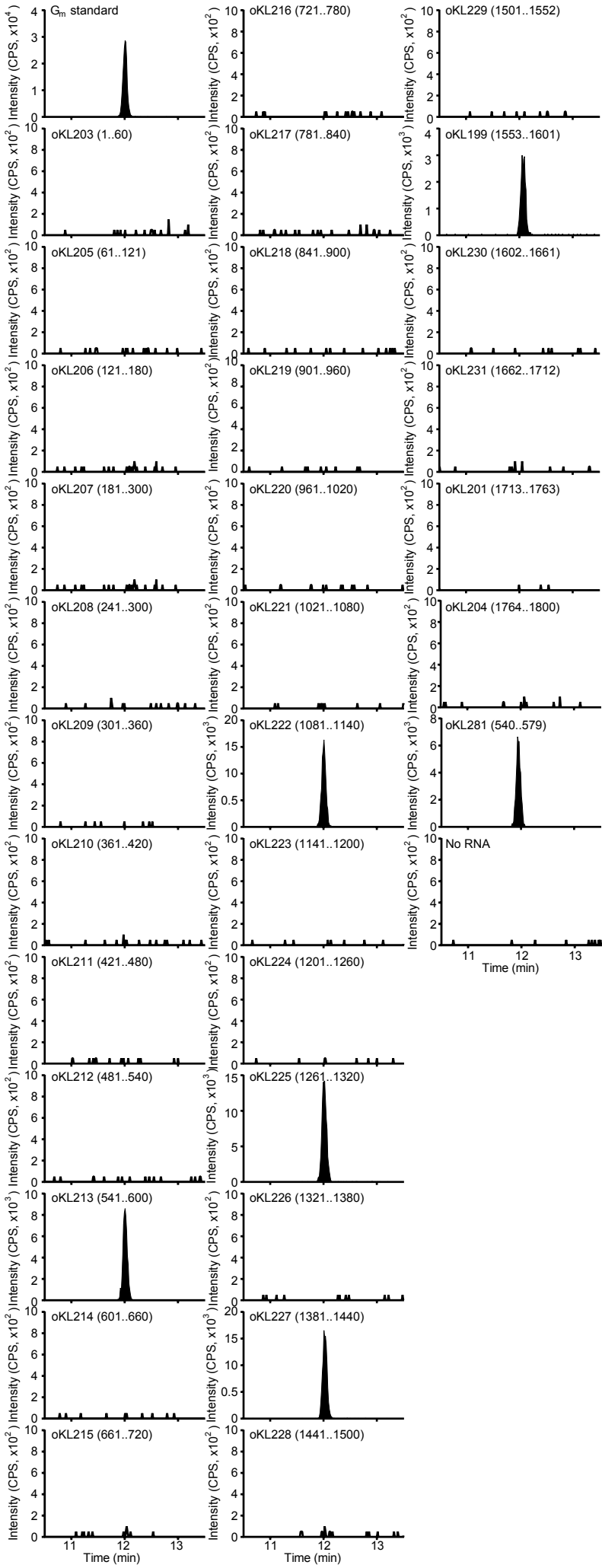
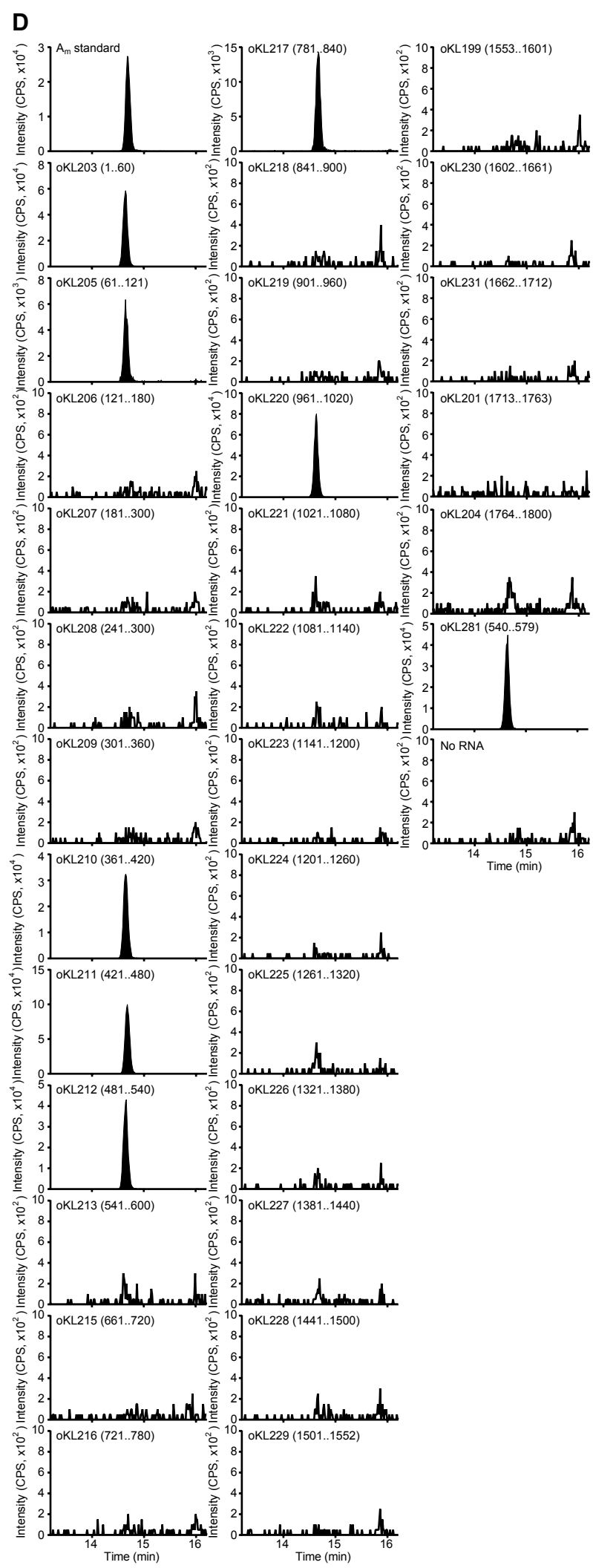
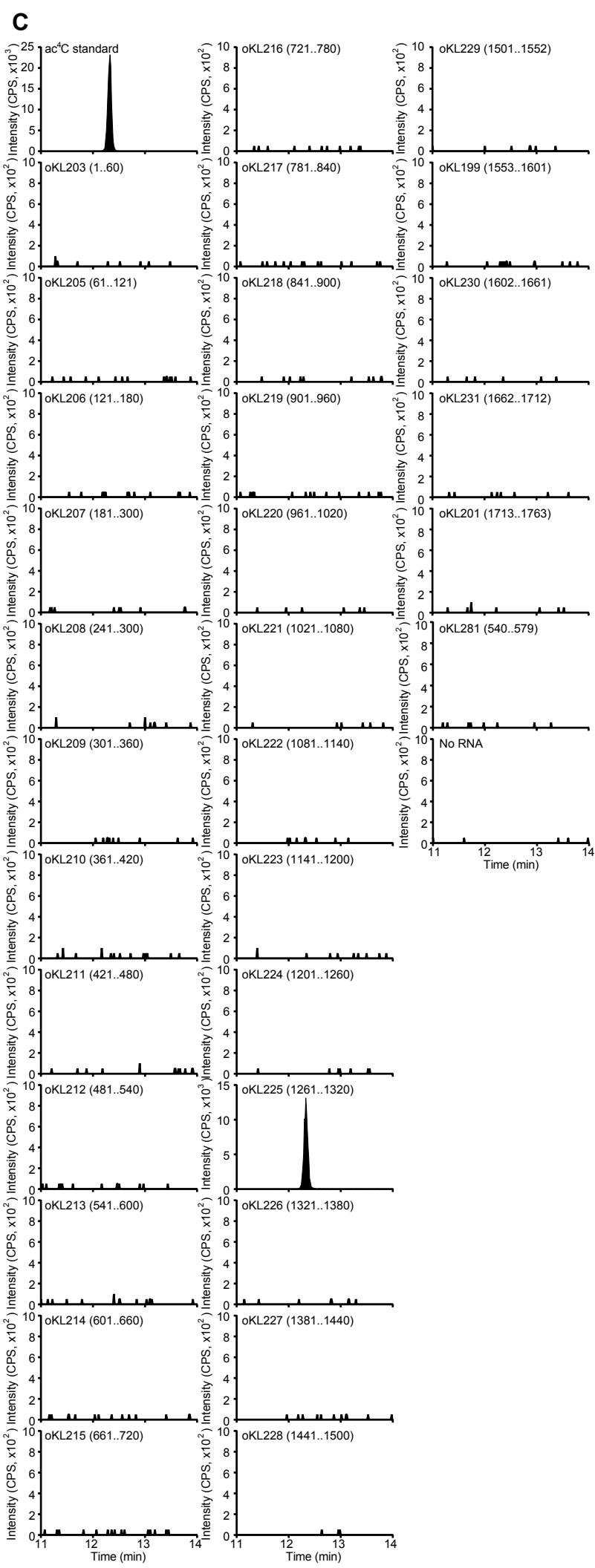
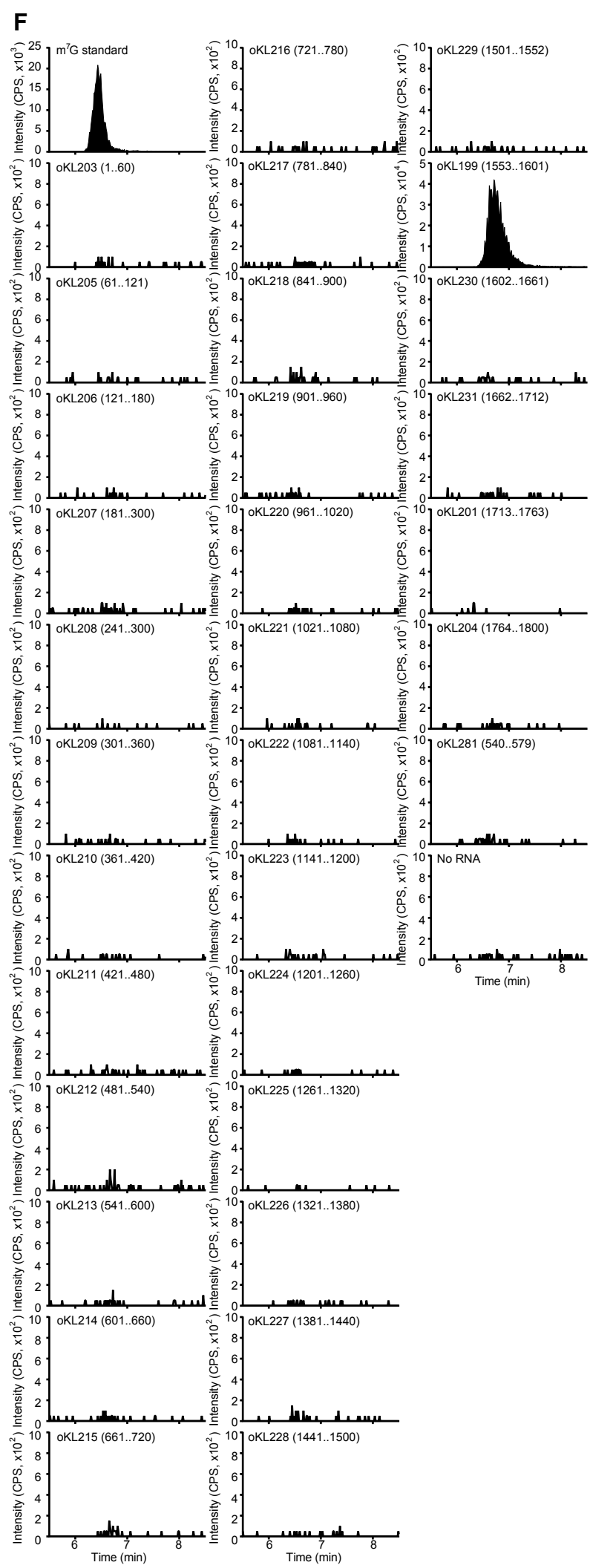
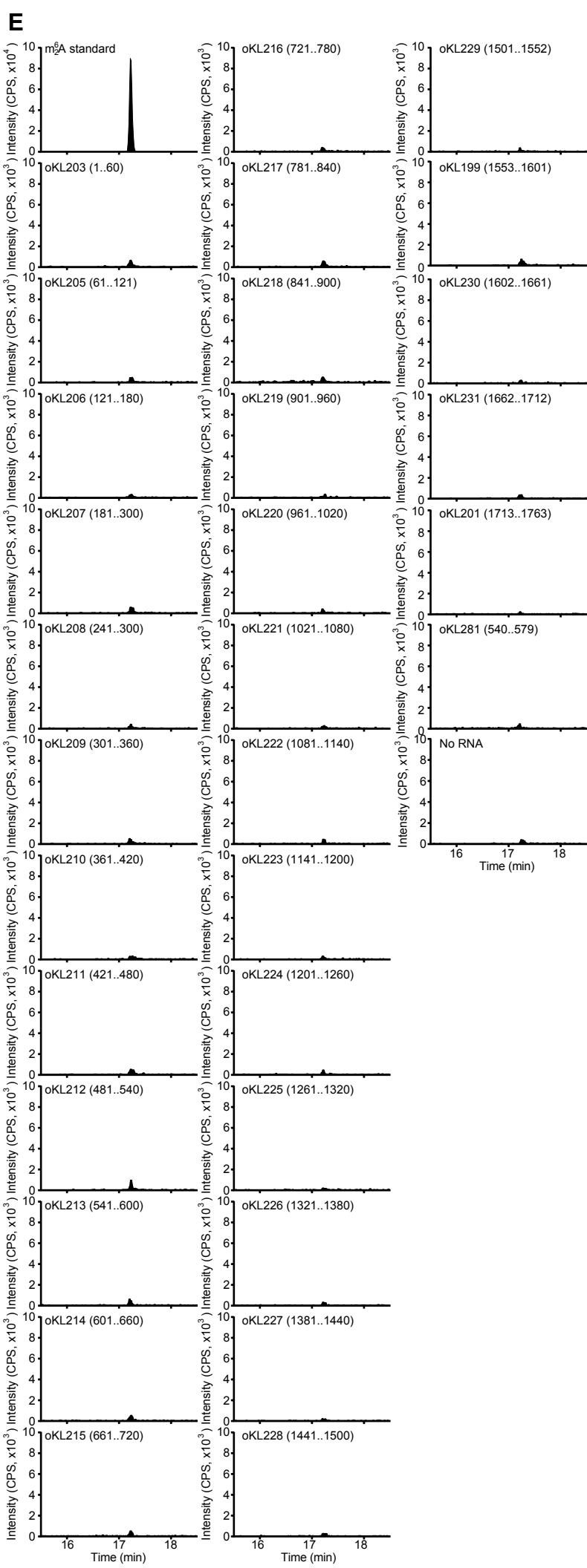


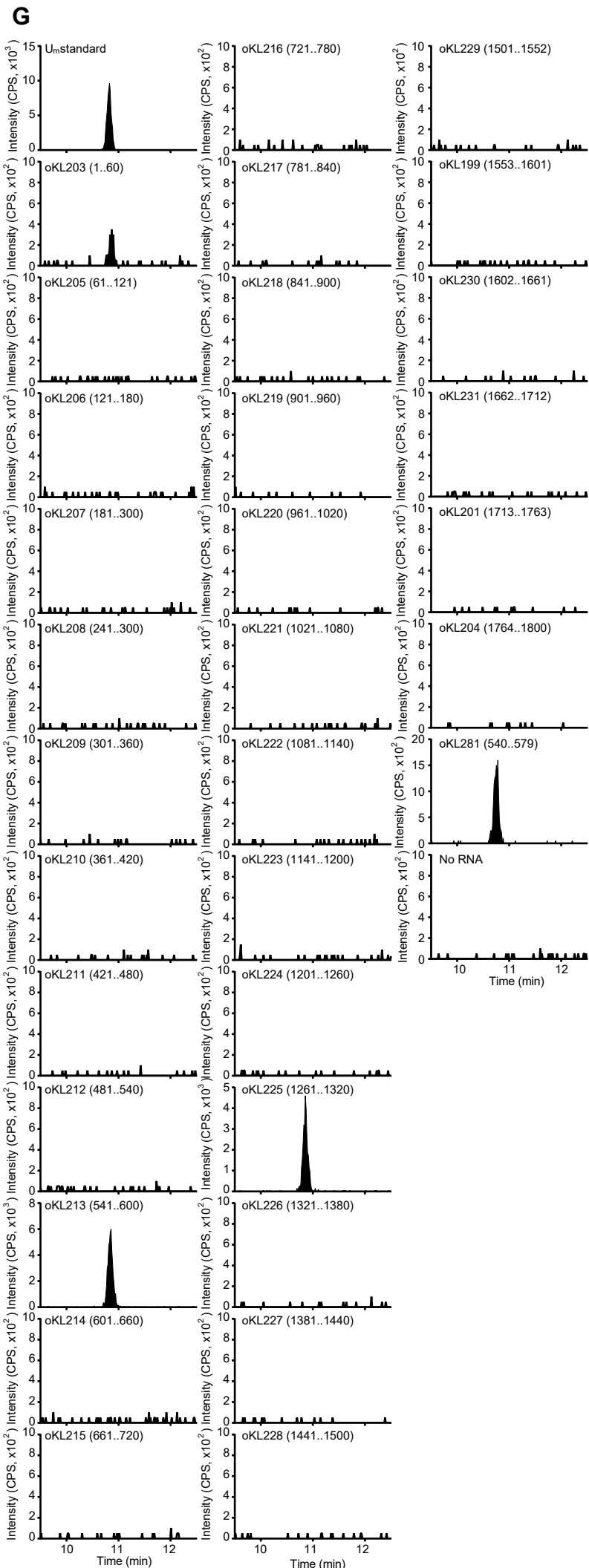
Figure S8. Characterization of *dim1* mutants. Related to Figures 3 and 5.

(A) The E85Q mutant grows slightly more slowly under nutrient replete condition. Cells were grown in SFM medium to log phase and washed with sterile water. Cells were adjusted to a final OD_{600} of 0.5 and serially diluted in water, before being plated onto an SD agar plate. (B) Levels of amino acids in *dim1* mutants under methionine-replete and -starvation conditions. Mean \pm s.d. ($n = 2$ biological replicates). (C) Examination of rRNA processing in *tsr3* Δ mutant using Northern blot. Cells were grown in SFM and collected for Northern blot as described in STAR METHODS. (D) Changes in modified nucleosides in 18S rRNA. Cells were grown in SFM and shifted to SF for 2 h. 18S rRNA was isolated, digested, and analyzed by LC-MS/MS as described in STAR METHODS. Peak area of modified nucleosides was first normalized to that of adenosine and to WT with methionine. m^6A and m^2A from the E85Q mutant were at background levels and thus not shown. Mean \pm s.d. ($n = 2$ biological replicates).

A**B**







Data S1. Chromatograms of MBN protection assay targeting m^6A (A), G_m (B), ac^cC (C), A_m (D), m_2^6A (E), m^7G (F), and U_m (G). Related to Figure 1. All the modified nucleosides were detected in the expected regions of 18S rRNA according to Taoka et al. (2016). It should be noted that the A_m modification at 541 was not detected in oKL213-protected region (541..600), but in oKL212-protected region (481..540) and oKL281-protected region (540..579). This discrepancy is likely due to the imprecise trimming of the corresponding RNA/DNA ends in MBN protection assay.

Table S4. Strains, plasmids, antibodies, and primers. Related to START METHODS.

Strains		
Name	Genotype	References
WT ^a	<i>MATa</i> CEN.PK	(van Dijken et al., 2000)
KL139	<i>MATa/α</i> CEN.PK	(van Dijken et al., 2000)
S288C	<i>MATα</i> <i>SUC2 mal mel gal2 CUP1 flo1 flo8-1 hap1</i>	ATCC®204508
W303	<i>MATa bud4Δ::BUD4(S288C) can1-100</i>	(Korolev et al., 2012)
WT ^b	<i>MATa ho:: kanMX6-DIM1 dim1:: hygMX6</i>	This work
E85Q	<i>MATa ho:: kanMX6-dim1^{E85Q} dim1:: hygMX6</i>	This work
E85D	<i>MATa ho:: kanMX6-dim1^{E85D} dim1:: hygMX6</i>	This work
D87E	<i>MATa ho:: kanMX6-dim1^{D87E} dim1:: hygMX6</i>	This work
E85D D87E	<i>MATa ho:: kanMX6-dim1^{E85D D87E} dim1:: hygMX6</i>	This work
E85A	<i>MATa ho:: kanMX6-dim1^{E85A} dim1:: hygMX6</i>	This work
E85W	<i>MATa ho:: kanMX6-dim1^{E85W} dim1:: hygMX6</i>	This work
E85F	<i>MATa ho:: kanMX6-dim1^{E85F} dim1:: hygMX6</i>	This work
E85Y	<i>MATa ho:: kanMX6-dim1^{E85Y} dim1:: hygMX6</i>	This work
E85C	<i>MATa ho:: kanMX6-dim1^{E85C} dim1:: hygMX6</i>	This work
E85G	<i>MATa ho:: kanMX6-dim1^{E85G} dim1:: hygMX6</i>	This work
E85V	<i>MATa ho:: kanMX6-dim1^{E85V} dim1:: hygMX6</i>	This work
E85I	<i>MATa ho:: kanMX6-dim1^{E85I} dim1:: hygMX6</i>	This work
E85L	<i>MATa ho:: kanMX6-dim1^{E85L} dim1:: hygMX6</i>	This work
E85S	<i>MATa ho:: kanMX6-dim1^{E85S} dim1:: hygMX6</i>	This work
E85T	<i>MATa ho:: kanMX6-dim1^{E85T} dim1:: hygMX6</i>	This work
E85N	<i>MATa ho:: kanMX6-dim1^{E85N} dim1:: hygMX6</i>	This work
E85K	<i>MATa ho:: kanMX6-dim1^{E85K} dim1:: hygMX6</i>	This work
E85R	<i>MATa ho:: kanMX6-dim1^{E85R} dim1:: hygMX6</i>	This work
E85P	<i>MATa ho:: kanMX6-dim1^{E85P} dim1:: hygMX6</i>	This work
E85M	<i>MATa ho:: kanMX6-dim1^{E85M} dim1:: hygMX6</i>	This work
E85H	<i>MATa ho:: kanMX6-dim1^{E85H} dim1:: hygMX6</i>	This work
<i>sam1Δ sam2Δ</i>	<i>MATa sam1::kanMX6 sam2::hygMX6</i>	This work
WT- <i>lacZ</i>	<i>MATa ho::kanMX6-DIM1 dim1::hygMX6 x2::Ptef1-Ec lacZ-Tcyc1-natMX6⁶</i>	This work
E85D- <i>lacZ</i>	<i>MATa ho::kanMX6-dim1^{E85D} dim1::hygMX6 x2::Ptef1-Ec lacZ-Tcyc1-natMX6⁶</i>	This work
E85Q- <i>lacZ</i>	<i>MATa ho::kanMX6-dim1^{E85Q} dim1::hygMX6 x2::Ptef1-Ec lacZ-Tcyc1-natMX6⁶</i>	This work
D87E- <i>lacZ</i>	<i>MATa ho::kanMX6-dim1^{D87E} dim1::hygMX6 x2::Ptef1-Ec lacZ-Tcyc1-natMX6⁶</i>	This work
WT-FLAG	<i>MATa ho:: kanMX6-DIM1-FLAG dim1::hygMX6</i>	This work
E85D-FLAG	<i>MATa ho:: kanMX6-dim1^{E85D}-FLAG dim1:: hygMX6</i>	This work
D87E-FLAG	<i>MATa ho:: kanMX6-dim1^{D87E}-FLAG dim1:: hygMX6</i>	This work
E85Q-FLAG	<i>MATa ho:: kanMX6-dim1^{E85Q}-FLAG dim1:: hygMX6</i>	This work
<i>gcd14Δ IMT4 OE</i>	<i>MATa gcd14::hygMX6 2 micron-IMT4-kanMX6</i>	This work
<i>rrp8Δ ybr141cΔ</i>	<i>MATa rrp8::kanMX6 ybr141c::hygMX6</i>	This work
WT <i>rps22B-3×FLAG</i>	<i>MATa ho:: kanMX6-DIM1 dim1:: hygMX6 rps22B::3×FLAG-natMX6</i>	This work
E85Q <i>rps22B-3×FLAG</i>	<i>MATa ho:: kanMX6-dim1^{E85Q} dim1:: hygMX6 rps22B::3×FLAG-natMX6</i>	This work
WT <i>rps9A-3×FLAG</i>	<i>MATa ho:: kanMX6-DIM1 dim1:: hygMX6 rps9A::3×FLAG-natMX6</i>	This work
E85Q <i>rps9A-3×FLAG</i>	<i>MATa ho:: kanMX6-dim1^{E85Q} dim1:: hygMX6 rps9A::3×FLAG-natMX6</i>	This work
<i>rps22BΔ pKL23 (H245R)</i>	<i>MATa ho:: kanMX6-DIM1 dim1:: hygMX6 rps22B::natMX6 ura3:: Sh ble pKL23</i>	This work
<i>rps22BΔ pKL24 (control)</i>	<i>MATa ho:: kanMX6-DIM1 dim1:: hygMX6 rps22B::natMX6 ura3:: Sh ble pKL24</i>	This work
<i>rps9AΔ pKL23 (H245R)</i>	<i>MATa ho:: kanMX6-DIM1 dim1:: hygMX6 rps9A::natMX6 ura3:: Sh ble pKL23</i>	This work
<i>rps9AΔ pKL24 (control)</i>	<i>MATa ho:: kanMX6-DIM1 dim1:: hygMX6 rps9A::natMX6 ura3:: Sh ble pKL24</i>	This work
WT pKL23 (H245R)	<i>MATa ho:: kanMX6-DIM1 dim1:: hygMX6 ura3:: natMX6 pKL23</i>	This work
E85Q pKL23 (H245R)	<i>MATa ho:: kanMX6-dim1^{E85Q} dim1:: hygMX6 ura3:: natMX6 pKL23</i>	This work
D87E pKL23 (H245R)	<i>MATa ho:: kanMX6-dim1^{D87E} dim1:: hygMX6 ura3:: natMX6 pKL23</i>	This work
WT pKL24 (control)	<i>MATa ho:: kanMX6-DIM1 dim1:: hygMX6 ura3:: natMX6 pKL24</i>	This work
E85Q pKL24 (control)	<i>MATa ho:: kanMX6-dim1^{E85Q} dim1:: hygMX6 ura3:: natMX6 pKL24</i>	This work
D87E pKL24 (control)	<i>MATa ho:: kanMX6-dim1^{D87E} dim1:: hygMX6 ura3:: natMX6 pKL24</i>	This work
<i>tsr3Δ pKL23 (H245R)</i>	<i>MATa ho:: kanMX6-DIM1 dim1:: hygMX6 tsr3::natMX6 ura3:: Sh ble pKL23</i>	This work
<i>tsr3Δ pKL24 (control)</i>	<i>MATa ho:: kanMX6-DIM1 dim1:: hygMX6 tsr3::natMX6 ura3:: Sh ble pKL24</i>	This work
Plasmids		
Name	Description	References
pFA6a- <i>hphMX6</i>	To replace a gene of interest with the <i>hphMX6</i> gene	(Longtine et al., 1998)
pFA6a- <i>kanMX6</i>	To replace a gene of interest with the <i>kanMX6</i> gene	(Longtine et al., 1998)

pFA6a-natMX6	To replace a gene of interest with the <i>natMX6</i> gene	(Longtine et al., 1998)
pUG66	To replace a gene of interest with the <i>Sh ble</i> gene	(Gueldener et al., 2002)
<i>HO-kanMX6-HO</i>	To ectopically express a gene of interest at the <i>HO</i> locus	(Voth et al., 2001)
Control (aka. pDB722 or pKL24)	Control Dual-Luciferase reporter	(Keeling et al., 2004)
H245R (aka. pDB868 or pKL23)	Dual-Luciferase reporter for miscoding	(Salas-Marco and Bedwell, 2005)
2 micron <i>IMT4-kanMX6</i>	To express <i>IMT4</i> with its 5' (~500 bp) and 3' (~300 bp) UTRs on a 2 micron plasmid	This work
<i>HO-kanMX6-DIM1-HO</i>	To ectopically express <i>DIM1</i> with its 5' (~500 bp) and 3' (~300 bp) UTRs	This work
<i>HO-kanMX6-dim1^{ES5A}-HO</i>	To ectopically express <i>dim1^{ES5A}</i> with its 5' (~500 bp) and 3' (~300 bp) UTRs	This work
<i>HO-kanMX6-dim1^{ES5G}-HO</i>	To ectopically express <i>dim1^{ES5G}</i> with its 5' (~500 bp) and 3' (~300 bp) UTRs	This work
<i>HO-kanMX6-dim1^{ES5D}-HO</i>	To ectopically express <i>dim1^{ES5D}</i> with its 5' (~500 bp) and 3' (~300 bp) UTRs	This work
<i>HO-kanMX6-dim1^{ES5V}-HO</i>	To ectopically express <i>dim1^{ES5V}</i> with its 5' (~500 bp) and 3' (~300 bp) UTRs	This work
<i>HO-kanMX6-dim1^{ES5R}-HO</i>	To ectopically express <i>dim1^{ES5R}</i> with its 5' (~500 bp) and 3' (~300 bp) UTRs	This work
<i>HO-kanMX6-dim1^{ES5S}-HO</i>	To ectopically express <i>dim1^{ES5S}</i> with its 5' (~500 bp) and 3' (~300 bp) UTRs	This work
<i>HO-kanMX6-dim1^{ES5K}-HO</i>	To ectopically express <i>dim1^{ES5K}</i> with its 5' (~500 bp) and 3' (~300 bp) UTRs	This work
<i>HO-kanMX6-dim1^{ES5N}-HO</i>	To ectopically express <i>dim1^{ES5N}</i> with its 5' (~500 bp) and 3' (~300 bp) UTRs	This work
<i>HO-kanMX6-dim1^{ES5T}-HO</i>	To ectopically express <i>dim1^{ES5T}</i> with its 5' (~500 bp) and 3' (~300 bp) UTRs	This work
<i>HO-kanMX6-dim1^{ES5M}-HO</i>	To ectopically express <i>dim1^{ES5M}</i> with its 5' (~500 bp) and 3' (~300 bp) UTRs	This work
<i>HO-kanMX6-dim1^{ES5I}-HO</i>	To ectopically express <i>dim1^{ES5I}</i> with its 5' (~500 bp) and 3' (~300 bp) UTRs	This work
<i>HO-kanMX6-dim1^{ES5Q}-HO</i>	To ectopically express <i>dim1^{ES5Q}</i> with its 5' (~500 bp) and 3' (~300 bp) UTRs	This work
<i>HO-kanMX6-dim1^{ES5H}-HO</i>	To ectopically express <i>dim1^{ES5H}</i> with its 5' (~500 bp) and 3' (~300 bp) UTRs	This work
<i>HO-kanMX6-dim1^{ES5P}-HO</i>	To ectopically express <i>dim1^{ES5P}</i> with its 5' (~500 bp) and 3' (~300 bp) UTRs	This work
<i>HO-kanMX6-dim1^{ES5L}-HO</i>	To ectopically express <i>dim1^{ES5L}</i> with its 5' (~500 bp) and 3' (~300 bp) UTRs	This work
<i>HO-kanMX6-dim1^{ES5C}-HO</i>	To ectopically express <i>dim1^{ES5C}</i> with its 5' (~500 bp) and 3' (~300 bp) UTRs	This work
<i>HO-kanMX6-dim1^{ES5Y}-HO</i>	To ectopically express <i>dim1^{ES5Y}</i> with its 5' (~500 bp) and 3' (~300 bp) UTRs	This work
<i>HO-kanMX6-dim1^{ES5F}-HO</i>	To ectopically express <i>dim1^{ES5F}</i> with its 5' (~500 bp) and 3' (~300 bp) UTRs	This work
<i>HO-kanMX6-dim1^{ES5W}-HO</i>	To ectopically express <i>dim1^{ES5W}</i> with its 5' (~500 bp) and 3' (~300 bp) UTRs	This work
<i>HO-kanMX6-dim1^{ES5D D87E}-HO</i>	To ectopically express <i>dim1^{ES5D D87E}</i> with its 5' (~500 bp) and 3' (~300 bp) UTRs	This work
<i>HO-kanMX6-dim1^{D87E}-HO</i>	To ectopically express <i>dim1^{D87E}</i> with its 5' (~500 bp) and 3' (~300 bp) UTRs	This work
<i>HO-kanMX6-DIM1-FLAG-HO</i>	To ectopically express <i>DIM1-FLAG</i> with its 5' (~500 bp) and 3' (~300 bp) UTRs	This work
<i>HO-kanMX6-dim1^{ES5D}-FLAG-HO</i>	To ectopically express <i>dim1^{ES5D}-FLAG</i> with its 5' (~500 bp) and 3' (~300 bp) UTRs	This work
<i>HO-kanMX6-dim1^{ES5Q}-FLAG-HO</i>	To ectopically express <i>dim1^{ES5Q}-FLAG</i> with its 5' (~500 bp) and 3' (~300 bp) UTRs	This work
<i>HO-kanMX6-dim1^{D87E}-FLAG-HO</i>	To ectopically express <i>dim1^{D87E}-FLAG</i> with its 5' (~500 bp) and 3' (~300 bp) UTRs	This work
p417-P _{TEF1} -lacZ-T _{CYC1} -natMX6	To express <i>Escherichia coli lacZ</i>	This work

Antibodies

Name	Description	Cat. #
α -FLAG	To detect the FLAG epitope	Sigma F1804
α -G6pdh	To detect G6pdh	Sigma A9521
α -Rpn10	To detect Rpn10p	Abcam ab98843

Primers

Name	Sequence (5' to 3')	Note
oKL169	ATCCCCGGGTTAATTAAGGCGCGCCAGATCTGTTTAGCTTGCCTCGTCCC	
oKL203	AGACATGCATGGCTTAATCTTTGAGACAAGCATATGACTACTGGCAGGATCAACCAGATA	1..60 ^d
oKL205	ATAAACGATAACTGATTTAATGAGCCATTCGCAGTTTCACTGTATAAATTGCTTATACTT	61..120 ^d
oKL206	TTAAGCATGTATTAGCTCTAGAATTACCACAGTTATACCATGTAGTAAAGGAACATCAA	121..180 ^d
oKL207	AGAGTCCGAAGACATTGATTTTTTATCTAATAAAATACATCTCTCCAAAGGGTTCGAGATT	181..240 ^d
oKL208	TTGAATGAACCATCGCCAGCACAAAGGCCATGCGATTCGAAAAGTTATTATGAATCATCAA	241..300 ^d
oKL209	TTACCCGTTGAAACCATGGTAGGCCACTATCCTACCATCGAAAAGTTGATAGGCCAGAAAT	301..360 ^d
oKL210	TCCTTGGATGTGGTAGCCGTTTCTCAGGCTCCCTCTCCGGAATCGAACCCCTTATTCCCCG	361..420 ^d
oKL211	CGTTATTTATTGTCACTACCTCCCTGAATTAGGATTGGGTAATTTGCGCGCCTGCTGCCT	421..480 ^d
oKL212	CCTCGTTAAGGTATTTACATTGTACTCATTCCAATTACAAGACCCGAATGGGCCCTGTAT	481..540 ^d
oKL213	ATACGCTATTGGAGCTGGAATTACCGCGGCTGCTGGCACCAGACTTGCCCTCCAATTGTT	541..600 ^d
oKL214	CGGACCGGCCAACCCGGGCCCAAAGTTCAACTACGAGCTTTTTAACTGCAACAACCTTAAT	601..660 ^d
oKL215	CAAGGACTCAAGGTTAGCCAGAAGGAAAGCCCGTTGGAAATCCAGTACACGAAAAAAT	661..720 ^d
oKL216	TACGCTGCTTTGAACACTCTAATTTTTCAAAGTAAAGTCTGTTTCGCCAAGAGCCA	721..780 ^d
oKL217	AACCAACAAAATAGAACCAAAAGTCTTATTCTATTATTCCATGCTAATATATTTCGAGCAA	781..840 ^d
oKL218	TCTGACAATTGAATACTGATGCCCCGACCGTCCCTATTAATCATTACGATGGTCTTAGA	841..900 ^d
oKL219	AAACGTCCTTGGCAAATGCTTTCGCAGTAGTTAGTCTTCAATAAAATCCAAGAATTTACC	901..960 ^d
oKL220	TTAAGACTACGACGGTATCTGATCATCTCGATCCCCTAATTTTCGTTCTTGATTAATGA	961..1020 ^d
oKL221	AAGGTGCCGAGTGGGTCATTAATAAAAAACACCACCCGATCCCTAGTCGGCATAGTTTATGG	1021..1080 ^d
oKL222	CTTTAAGTTTCAGCCTTGCACCATACTCCCCCAGAACCCAAAGACTTTGATTTCTCGT	1081..1140 ^d
oKL223	CCCGTGTGAGTCAAATTAAGCCGAGGCTCCACTCCTGGTGGTGCCTTCCGTCAATTC	1141..1200 ^d

oKL224	AAAATCAAGAAAGAGCTCTCAATCTGTCAATCCTTATTGTGTCTGGACCTGGTGAGTTTC	1201..1260 ^d
oKL225	ATCGCAATTAAGCAGACAAATCACTCCACCAACTAAGAACGGCCATGCACCACCACCCAC	1261..1320 ^d
oKL226	AGAAGTGGATAACCAGCAAATGCTAGCACCCTATTTAGTAGGTTAAGGTCTCGTTCGGT	1321..1380 ^d
oKL227	GGCATCACAGACCTGTTATTGCCCTCAAACCTCCATCGGCTTGAAACCGATAGTCCCTCTA	1381..1440 ^d
oKL228	GCCAAGGTTAGACTCGCTGGCTCCGTCAGTGTAGCGCGCGTGGCGCCGAGAACGCTCTAAG	1441..1500 ^d
oKL229	AATGCTCTATCCCCAGCACGACGGAGTTTCACAAGATTACCAAGACCTCTCG	1501..1552 ^d
oKL199	CTGATGACTTGGCGTTACTAGGAATTCCTCGTTGAAGAGCAATAATTAC	1553..1601 ^d
oKL230	ATTCAATCGGTACTAGCGACGGGCGGTGTGTACAAAGGGCAGGGACGTAATCAACGCAAG	1602..1661 ^d
oKL231	TGAGATGGAGTTGCCCCCTTCTAAGCAGATCCTGAGGCCTCACTAAGCC	1662..1712 ^d
oKL201	TTACGACTTTTAGTTCCTCTAAATGACCAAGTTTGTCCAAATTCTCCGCTC	1713..1763 ^d
oKL204	TAATGATCCTTCCGCAGGTTACCTACGGAAACCTTG	1764..1800 ^d
oKL235	CCTACGGAAACCTTGTTACGACTTTTAGTTCTCTAAATGACCAAGTTTG	1729..1778 ^d
oKL236	TCACCTACGGAAACCTTGTTACGACTTTTAGTTCTCTAAATGACCAAGTTTG	1729..1781 ^d
oKL237	TTCACCTACGGAAACCTTGTTACGACTTTTAGTTCTCTAAATGACCAAGTTTG	1729..1782 ^d
oKL242	TCCGCAGGTTACCTACGGAAACCTTGTTACGACTTTTAGTTCTCTAAATGACCAAGTTTG	1729..1790 ^d
oKL243	TTCCGCAGGTTACCTACGGAAACCTTGTTACGACTTTTAGTTCTCTAAATGACCAAGTTTG	1729..1791 ^d
oKL246	TAATGATCCTTCCGCAGGTTACCTACGGAAACCTTGTTACGACTTTTAGTTCTCTAAATGACCAAGTTTG	1729..1800 ^d
oKL261	GCAAAAAACGTAGTGGCAGTAGCAATGGATCCCAGAATGGCTGC ^e	<i>dim1</i> ^{E85A} (f)
oKL262	GCAGCCATTCTGGGATCCATTGCTACTGCCACTACGTTTTTTGC	<i>dim1</i> ^{E85A} (r)
oKL506	AACGTAGTGGCAGTATGGATGGATCCCAGAATG ^e	<i>dim1</i> ^{E85W} (f)
oKL507	CATTCTGGGATCCATCCACTGCCACTACGTT	<i>dim1</i> ^{E85W} (r)
oKL625	AACGTAGTGGCAGTAGGTATGGATCCCAGAATG ^e	<i>dim1</i> ^{E85G} (f)
oKL626	CATTCTGGGATCCATACTACTGCCACTACGTT	<i>dim1</i> ^{E85G} (r)
oKL627	AACGTAGTGGCAGTAGATATGGATCCCAGAATG ^e	<i>dim1</i> ^{E85D} (f)
oKL628	CATTCTGGGATCCATATCTACTGCCACTACGTT	<i>dim1</i> ^{E85D} (r)
oKL629	AACGTAGTGGCAGTAGTTATGGATCCCAGAATG ^e	<i>dim1</i> ^{E85V} (f)
oKL630	CATTCTGGGATCCATAACTACTGCCACTACGTT	<i>dim1</i> ^{E85V} (r)
oKL631	AACGTAGTGGCAGTAAAGAATGGATCCCAGAATG ^e	<i>dim1</i> ^{E85R} (f)
oKL632	CATTCTGGGATCCATTCTTACTGCCACTACGTT	<i>dim1</i> ^{E85R} (r)
oKL633	AACGTAGTGGCAGTATCTATGGATCCCAGAATG ^e	<i>dim1</i> ^{E85S} (f)
oKL634	CATTCTGGGATCCATAGATACTGCCACTACGTT	<i>dim1</i> ^{E85S} (r)
oKL635	AACGTAGTGGCAGTAAAATGGATCCCAGAATG ^e	<i>dim1</i> ^{E85K} (f)
oKL636	CATTCTGGGATCCATTTTTACTGCCACTACGTT	<i>dim1</i> ^{E85K} (r)
oKL637	AACGTAGTGGCAGTAAATATGGATCCCAGAATG ^e	<i>dim1</i> ^{E85N} (f)
oKL638	CATTCTGGGATCCATATTTACTGCCACTACGTT	<i>dim1</i> ^{E85N} (r)
oKL639	AACGTAGTGGCAGTAACTATGGATCCCAGAATG ^e	<i>dim1</i> ^{E85T} (f)
oKL640	CATTCTGGGATCCATAGTTACTGCCACTACGTT	<i>dim1</i> ^{E85T} (r)
oKL641	AACGTAGTGGCAGTAAATGATGGATCCCAGAATG ^e	<i>dim1</i> ^{E85M} (f)
oKL642	CATTCTGGGATCCATCATTACTGCCACTACGTT	<i>dim1</i> ^{E85M} (r)
oKL643	AACGTAGTGGCAGTAAATATGGATCCCAGAATG ^e	<i>dim1</i> ^{E85I} (f)
oKL644	CATTCTGGGATCCATAATTACTGCCACTACGTT	<i>dim1</i> ^{E85I} (r)
oKL645	AACGTAGTGGCAGTACAAATGGATCCCAGAATG ^e	<i>dim1</i> ^{E85Q} (f)
oKL646	CATTCTGGGATCCATTTGTACTGCCACTACGTT	<i>dim1</i> ^{E85Q} (r)
oKL647	AACGTAGTGGCAGTACATATGGATCCCAGAATG ^e	<i>dim1</i> ^{E85H} (f)
oKL648	CATTCTGGGATCCATATGTACTGCCACTACGTT	<i>dim1</i> ^{E85H} (r)
oKL649	AACGTAGTGGCAGTACCAATGGATCCCAGAATG ^e	<i>dim1</i> ^{E85P} (f)
oKL650	CATTCTGGGATCCATTGGTACTGCCACTACGTT	<i>dim1</i> ^{E85P} (r)
oKL651	AACGTAGTGGCAGTATTGATGGATCCCAGAATG ^e	<i>dim1</i> ^{E85L} (f)
oKL652	CATTCTGGGATCCATCAATACTGCCACTACGTT	<i>dim1</i> ^{E85L} (r)
oKL653	AACGTAGTGGCAGTATGTTATGGATCCCAGAATG ^e	<i>dim1</i> ^{E85C} (f)
oKL654	CATTCTGGGATCCATACATACTGCCACTACGTT	<i>dim1</i> ^{E85C} (r)
oKL655	AACGTAGTGGCAGTATATATGGATCCCAGAATG ^e	<i>dim1</i> ^{E85Y} (f)
oKL656	CATTCTGGGATCCATATATACTGCCACTACGTT	<i>dim1</i> ^{E85Y} (r)
oKL657	AACGTAGTGGCAGTATTTATGGATCCCAGAATG ^e	<i>dim1</i> ^{E85F} (f)
oKL658	CATTCTGGGATCCATAAAATACTGCCACTACGTT	<i>dim1</i> ^{E85F} (r)
oKL700	GTGGCAGTAGAAAATGGAACCCAGAATGGCTGCA ^e	<i>dim1</i> ^{D87E} (f)
oKL701	TGCAGCCATTCTGGGTTCCATTTCTACTGCCAC	<i>dim1</i> ^{D87E} (r)
oKL698	GTGGCAGTAGATATGGAACCCAGAATGGCTGCA ^e	<i>dim1</i> ^{E85D,D87E} (f)
oKL699	TGCAGCCATTCTGGGTTCCATATCTACTGCCAC	<i>dim1</i> ^{E85D,D87E} (r)

Probes for Northern blot

Name	Sequence (5' to 3')	Target region
a	[btm]TACTTAGACATGCATGGCTTAATCTTTGAGACAAGCATATGACTACTGGC	yeast 18S rRNA

b	[btm]GACTCTCCATCTCTTGTCTTCTTGCCAGTAAAAGCTCTCATGCTCTTGC	yeast 20S pre-rRNA
c	[btm]CTCTGGGCCCCGATTGCTCGAATGCCCAAAGAAAAAGTTGCAAAGATATG	yeast ITS1 (A2&A3)
d	[btm]GTTACTAAGGCAATCCCGGTTGGTTCTTTTCCTCCGCTTATTGATATGC	yeast 25S rRNA
e	[btm]CCTCGCCCTCCGGGCTCCGTTAATGATCCT	Human ITS1

^aThis strain was used throughout this work except when mutant *dim1* strains were investigated.

^bThis strain was used only for comparison with mutant *dim1* strains.

^cThe *x2* site is the integration site for the *E. coli lacZ* gene on chromosome X, between *NCA3* and *ASF1*, precisely encompassing from 605 to 646 nucleotides upstream of the *NCA3* start codon. It was previously examined by Mikkelsen et al., who reported that ectopic expression at this site did not cause growth defects (Mikkelsen et al., 2012).

^dNumbers correspond to nucleotide positions in yeast 18S rRNA.

^eThe mutated codon is underlined in the forward primer. (f): forward primer; (r): reverse primer

Table S5. Medium formula^a. Related to STAR METHODS.

	complete	-C	-N	-P	-S (sulfur free)
salts (g L ⁻¹)					
CaCl ₂ •2H ₂ O	0.1	0.1	0.1	0.1	0.1
NaCl	0.1	0.1	0.1	0.1	0.1
MgCl ₂ •6H ₂ O	0.412	0.412	0.412	0.412	0.412
(NH ₄) ₂ SO ₄	5	5	0	5	0
Na ₂ SO ₄	0	0	5.4	0	0
NH ₄ Cl	0	0	0	0	4.05
KH ₂ PO ₄	1	1	1	0	1
KCl	0	0	0	0.55	0
metals (mg L ⁻¹)					
boric acid			0.5		
CuCl ₂ •2H ₂ O			0.0273		
KI			0.1		
FeCl ₃ •6H ₂ O			0.2		
MnCl ₂ •4H ₂ O			0.4684		
Na ₂ MoO ₄ •2H ₂ O			0.2		
ZnCl ₂ •H ₂ O			0.1895		
vitamins (mg L ⁻¹)					
biotin			0.002		
calcium pantothenate			0.4		
folic acid			0.002		
inositol			2		
niacin			0.4		
4-aminobenzoic acid			0.2		
pyridoxine HCl			0.4		
riboflavin			0.2		
thiamine-HCl			0.4		

^aFormula is based on Miller et al. (Miller et al., 2013) with sulfate ions replaced by chloride ions.

Table S6. MRM transitions for nucleosides and metabolites. Related to STAR METHODS.

Compounds	Q1	Q3	[U- ¹⁵ N]-Q1	[U- ¹⁵ N]-Q3
<i>N</i> ⁶ -methyladenosine (m ⁶ A)	282	150	287	155
<i>N</i> ⁴ -acetylcytidine (ac ⁴ C)	286	154	289	157
<i>N</i> ⁶ , <i>N</i> ⁶ -dimethyladenosine (m ⁶ ₂ A)	296	164	301	169
<i>N</i> ¹ -methyladenosine (m ¹ A)	282	150		
2'-O-methyladenosine (A _m)	282	136		
2'-O-methylguanosine (G _m)	298	152		
2'-O-methyluridine (U _m)	259	113		
<i>N</i> ⁷ -methylguanosine (m ⁷ G)	298	166		
adenosine	268	136		
cytidine	244	112		
uridine	245	113		
guanosine	284	152		
cysteine	122	59		
methionine	150	104		
homocysteine	136	90		
cystathionine	223	134		
SAM	399	250		
SAH	385	136		
GSH	308	179		
GSSG	613	355		
proline	116	70		
arginine	175	116		
histidine	156	110		
serine	106	60		
threonine/homoserine	120	74		
isoleucine	132	69		
(iso)leucine	132	86		
valine	118	55		
tryptophan	205	188		
phenylalanine	166	103		
tyrosine	182	136		